

A Direct Detection Search for Hidden Sector New Particles in the 3 - 60 MeV Mass Range

A. Ahmidouch, S. Davis, A. Gasparian (spokesperson, contact),
T. J. Hague (co-spokesperson), S. Mtingwa, R. Pedroni
North Carolina A&T State University, Greensboro, NC 27411

C. Ayerbe-Gayoso, H. Bhatt, D. Bhetuwal, T. Chetry, B. Devkota, J. Dunne,
D. Dutta (co-spokesperson), L. El Fassi, A. Karki, P. Mohanmurthy
Mississippi State University, Mississippi State, MS 39762

C. Peng (co-spokesperson)
Argonne National Lab, Lemont, IL 60439

S. Ali, X. Bai, J. Boyd, B. Dharmasena, V. Gamage, K. Gnanvo, S. Jeffas, S. Jian
N. Liyanage (co-spokesperson), J. Matter, H. Nguyen, A. Rathnayake
University of Virginia, Charlottesville, VA 22904

M. Khandaker
Energy Systems, Davis, CA 95616

D. Byer, H. Gao (co-spokesperson), B. Karki, V. Khachatryan, G. Matousek,
E. van Nieuwenhuizen, A. Smith, B. Yu, Z. Zhao, J. Zhou
Duke University, Durham, NC 27708

A. Shahinyan
Yerevan Physics Institute, Yerevan, Armenia

M. Battaglieri, D. Higinbotham, V. Kubarovsky, R. Paredes (co-spokesperson),
E. Pasyuk, S. Stepanyan, H. Avakian
Thomas Jefferson National Accelerator Facility, Newport News, VA 23606

A. Bianconi, G. Costantini, G. Gosta, M. Leali, S. Migliorati, L. Venturelli
*Dipartimento di Ingegneria dell'Informazione, Università di Brescia, Italy
and Istituto Nazionale di Fisica Nucleare, sezione di Pavia, Italy*

V. Mascagna
DiSAT, Università dell'Insubria, Como, Italy and INFN, sezione di Pavia, Italy

M. De Napoli
Istituto Nazionale di Fisica Nucleare, Sezione di Catania, Italy

M. Battaglieri, R. De Vita
Istituto Nazionale di Fisica Nucleare, Sezione di Genova, Genova, Italy

I. Larin, R. Miskimen
University of Massachusetts, Amherst, MA 01003

P. L. Cole
Lamar University, Beaumont, Texas 77710

W. Xiong
Syracuse University, Syracuse, New York 13244

Abstract

In our quest for investigating the nature of dark matter from the way its constituents interact with ordinary matter, we propose an experiment using a PbWO_4 calorimeter to search for or set new limits on the production rate of i) hidden sector dark matter mediator in the 3 – 60 MeV mass range via their e^+e^- decay (or $\gamma\gamma$ decay with limited tracking), and ii) the hypothetical X17 particle, claimed in two recent experiments. The search for these particles is motivated by new dark matter models and candidates introduced to account for the small-scale structure in astrophysical observations and anomalies such as the 4.2σ disagreement between experiments and the standard model prediction for the muon anomalous magnetic moment, and the excess of e^+e^- pairs from the ^8Be M1 nuclear transition to its ground state observed by the ATOMKI group. In these models the 1 – 100 MeV mass range is particularly well-motivated and the lower part of this range still remains unexplored. The proposed direct detection experiment will use a magnetic-spectrometer-free setup (the PRad apparatus) to detect all three final state particles in the visible decay of the dark matter mediator allowing for an effective control of the background and will cover the mass range in a single setting. The use of the well-demonstrated PRad setup allows for an essentially ready-to-run and uniquely cost-effective search for dark matter mediator in the 3 – 60 MeV mass range with a sensitivity of 7.2×10^{-8} - 5.9×10^{-9} to ϵ^2 the square of kinetic mixing interaction coupling constant. In the first appendix, we show an example of this type of analysis using the ^{12}C data from the PRad experiment. In the second appendix, we detail the additional work that was done after submitting this proposal before presenting at the JLab PAC49.

1 Executive Summary

We request 60 PAC days to perform a direct detection search for hidden sector particles in the 3–60 MeV mass range using the magnetic-spectrometer-free PRad setup in Hall-B. This experiment will exploit the well-demonstrated PRad setup to perform a ready-to-run and cost-effective search. This proposed search experiment is timely given the recent agreement between measurements of the muon $(g - 2)$ anomaly at BNL and FNAL as well as the 17-MeV particle proposed to account for the excess of e^+e^- pairs found in a nuclear transition in ^8Be from one of its 1^+ resonance to its ground state, and the electromagnetically forbidden M0 transition in ^4He . In particular, the 3 – 60 MeV mass range remains relatively unexplored amplifying the urgency.

The experiment will use 2.2 GeV and 3.3 GeV CW electron beams, with a current of 50 – 100 nA, on a 1 μm Ta foil placed in front of the PRad setup. All three final state particles- the scattered electron and the e^+e^- from the visible decay of the dark matter mediator - will be detected in the PbWO_4 part of the HyCal calorimeter. A pair of GEM chambers will be used to suppress the neutral background and events not originating from the target. This technique will help effectively suppress the background from the Bethe-Heitler process and provide a sensitivity of 7.2×10^{-8} - 5.9×10^{-9} to ϵ^2 , the square of the kinetic mixing interaction coupling constant. The $\epsilon^2 - m_X$ parameter space covered by this proposed experiment as shown below will help fill some of the void left by current, ongoing and other planned searches, thereby helping validate or placing limits on hidden sector dark matter models.

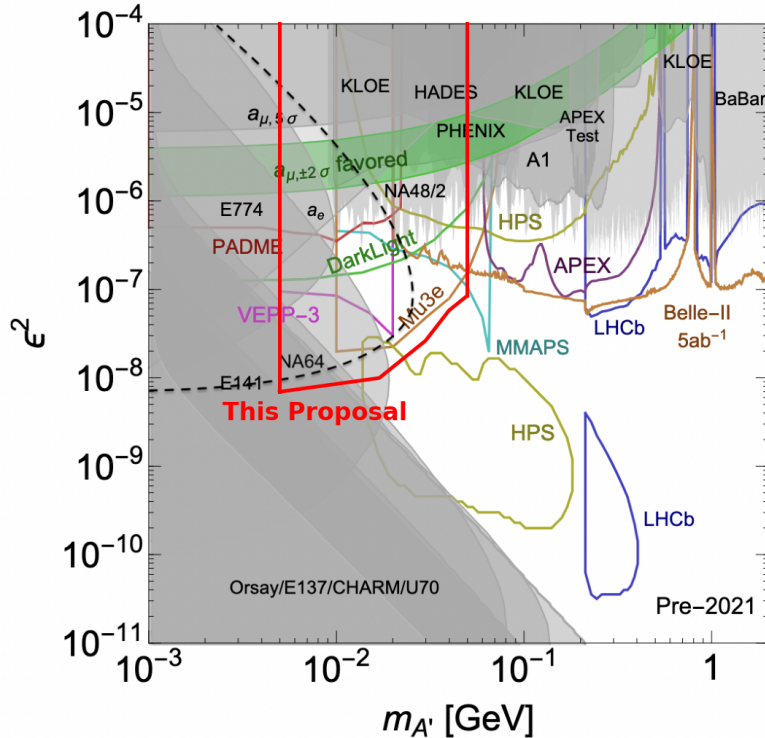


Figure 1: Projected coverage of the $\epsilon^2 - m_X$ parameter space by this proposal is shown by the thick red lines for the combined statistics of the two beam energies. Adapted from Ref. [1].

2 Introduction

The remarkable fact that $\sim 85\%$ of the matter in the Universe is of unknown origin - dark matter (DM) - is inferred from astronomical measurements over a wide range of distance scales, from the solar neighborhood to the largest cosmological scales. Yet, all of the evidence is essentially gravitational and does not provide direct information about the constituents of dark matter. Consequently, the investigation of the nature of DM, from its origin to its composition, and how its constituents interact with the ordinary matter, is one of the grand challenges in fundamental science. There are many candidate theories for dark matter and dark mediators that span a very large mass range, from 10^{-22} eV up to 100 solar masses. However, several recent observations and anomalies have brought forth new dark matter models and candidates such as the hidden sector dark matter (HSDM) [1] models that point to the $1 - 100$ MeV/ c^2 region as one that is of high priority to search [2]. In this proposal, we will describe an experiment that will search in the 3 - 60 MeV mass region for here-to-fore unobserved dark matter mediators. This experiment will utilize the bremsstrahlung-like production of a carrier of dark forces that subsequently decays to a e^+e^- or $\gamma\gamma$ pair (i.e. visible decays) which will be detected in the PRad setup with minimal modifications.

The availability of a high duty factor, high luminosity electron beam at Jefferson Lab provides an ideal setup to search for MeV-scale dark mediators with small coupling constants. The well tested PRad setup in Hall B will be used in this experiment to reach our physics goals. Using a magnetic-spectrometer-free setup allows the experiment to be sensitive to the full mass range in a single experimental setting, thus eliminating systematic uncertainties associated with field mapping or moving the spectrometer. The detection of all three final state particles in the PbWO_4 calorimeter along with tracking with GEM chambers allows for an effective control of the backgrounds. Moreover, it provides an essentially ready-to-run and uniquely cost effective search for DM particles in the 3 - 60 MeV mass range.

3 Physics Motivation

On large distance scales the structure of the Universe, inferred from cosmological data, is consistent with DM particles that are cold, collisionless, and interact with each other and with ordinary matter purely via gravity [3]. These cosmological data have converged on cold dark matter (CDM) as the standard model of cosmology [4] with weakly interacting massive particles (WIMP) as one of the primary DM candidates. Consequently, the search for the particle nature of DM had been focused on WIMPs. While WIMP dark matter remains highly motivated, a very significant parameter space for both WIMPs and models that realize WIMP dark matter have already been explored by recent searches [2]. To-date, the strongest bound to the WIMP-nucleon spin-independent elastic cross-section is posed by the XENON1T Experiment [5], which excludes values down to 4×10^{-47} cm². Clearly, new models and candidates are needed. Meanwhile, there are several astronomical observations and experimental anomalies that suggest the existence of an MeV-scale force-carrier connecting dark matter to standard model (SM) particles. Spurred on by these developments, new theoretical frameworks have been developed that are natural generalization of the WIMP idea but include interactions through a new force rather than just SM forces and yet retain many of the same attractive features of CDM [1].

In typical models, the new force carrier is a $U(1)$ gauge boson, or dark photon, henceforth referred to as X . The X can couple to SM matter via their electric charges. In the simplest schemes these couplings arise from a kinetic mixing interaction, $\frac{\epsilon}{2} F_{\mu\nu}^Y F'^{\mu\nu}$, where $F_{\mu\nu}^Y$ is the SM hypercharge field strength, $F'^{\mu\nu} = [\partial_\mu, X_\nu]$ is the dark gauge field, and ϵ is the dimensionless coupling constant of the X to SM matter. The X can acquire mass through the Higgs mechanism and a massive X will induce a charge on SM particles proportional to ϵ [6, 7]. In these models the MeV to GeV-scale X masses are found to be particularly well-motivated [7].

Recently, there has also been an increased interest in an X that does not couple proportionally to electric charge. Rather, the coupling is tied to flavor of quark or lepton. One such example is the protophobic X17 proposed in Ref. [8]. If an X were to have flavor-dependent couplings the parameter space for the X is more open than previously thought.

Here we will discuss a few primary motivators for DM searches in the sub-GeV mass range of the proposed experiment, and a more detailed discussion of dark sector searches can be found in Ref. [2].

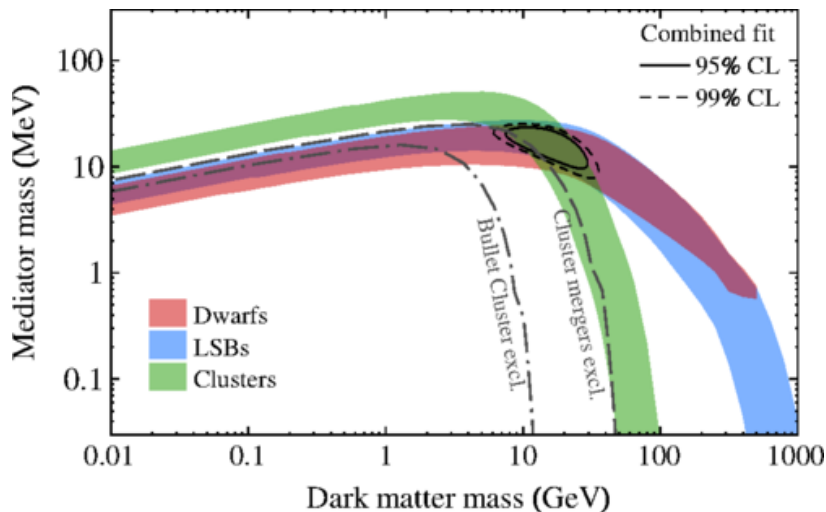


Figure 2: Parameter space for the dark photon model of self-interactions (with $\alpha' = \alpha_{EM}$), preferred by dwarfs (red), LSB spiral galaxies (blue), and clusters (green), each at 95% C.L. The combined 95% (99%) region is shown by the solid (dashed) contours. The estimated Bullet Cluster excluded region lies below the dot-dashed curve and the ensemble merging cluster excluded region below the long-dashed curve. Reproduced from Ref. [9].

3.1 Small Scale Structures in Astrophysical Observations

Since the 1990s there are a growing class of astrophysical observations at scales smaller than the virial radius of galaxies- collectively called small scale structures -that pose a challenge to the traditional weakly interacting CDM models [3]. However, dark matter models with significant self interactions, such as the hidden sector dark matter, are able to account for this small-scale puzzle while retaining the ability of CDM to describe the large scale structures. In order to be compatible with both small-scale and large-scale observations, the single particle mediated self interaction of the dark matter must be velocity dependent, and the favored mediator mass that is consistent with

all astrophysical observations lies in the $\sim 1 - 100$ MeV mass range, as shown in Fig. 2. Thus, in light of the observational evidence for small scale structure it is critical to explore the $\sim 1 - 100$ MeV mass range for possible dark sector mediator candidates.

3.2 Muon Anomalous Magnetic Moment

The Muon $g - 2$ collaboration has recently reported their measurement of the muon magnetic moment at Fermi National Accelerator Laboratory (FNAL) which is consistent with their previous measurement at Brookhaven National Laboratory (BNL) [10, 11]. These two results, with their uncertainties combined, show a 4.2σ deviation from the SM prediction. There are many proposed solutions to this discrepancy, here we will focus on potential MeV-scale bosons leading to loop corrections that can account for the muons' anomalous magnetic moment. For example the scalar Higgs doublet model which adds a second scalar doublet to the SM, resulting in a scalar sector with two Higgs doublets [12]. The muon couples directly to the new Z' gauge boson which can provide the required contribution to the muon $g - 2$. In fact, the Z' can be made very light with a sufficiently small coupling constant g' and can address the $(g - 2)_\mu$ anomaly with Z' mass roughly in the range of 10 -200 MeV [12], as shown in Fig. 3. In this model the DM is introduced via the DM mediated annihilations into the Z' . The DM relic abundance constrains the allowed phase space to near the Z' resonance, which implies $m_X \sim m_{Z'}/2$. If the Z' mass should lie around 10 - 200 MeV to explain the $(g - 2)_\mu$ the DM mass must lie in the mass range $m_X \approx 5 - 100$ MeV [12].

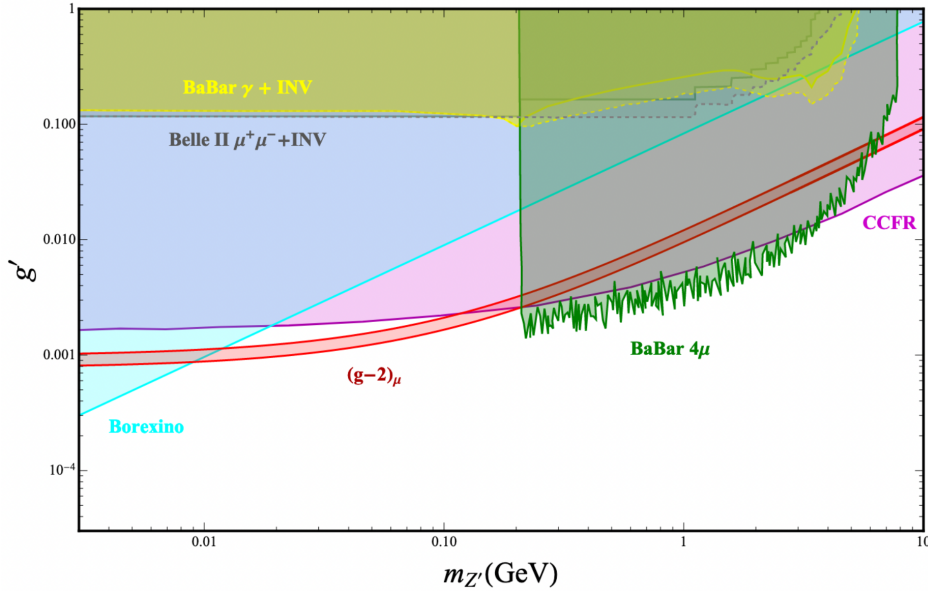


Figure 3: Allowed region to explain the $(g - 2)_\mu$ anomaly and exclusion regions on the Z' mass and gauge coupling constant g' from different experiments: e^+e^- colliders BABAR and Belle II; neutrino-electron scattering from Borexino, and neutrino trident production from the CCFR collaboration. These limits exclude most of the parameter space except for the region contained in the interval $10 \text{ MeV} < m_{Z'} < 200 \text{ MeV}$. This corresponds to a X mass of $5 \text{ MeV} < m_X < 100 \text{ MeV}$. Reproduced from Ref. [12].

The X can also directly contribute to the $(g - 2)_\mu$. The contributions of an X to the $(g - 2)_\mu$ scales as $1/m_X^2$, thus a smaller mass will have a comparably larger contribution than a higher mass particle. There have been numerous publications proposing dark photons in the MeV-range to, at a minimum, partially account for the muon anomalous magnetic moment [12, 13, 14, 15]. It is critical to search the MeV-scale region for a potential X to account for the observed muon $(g - 2)$ anomaly.

3.3 ATOMKI Beryllium Anomaly

A 1996 experiment [16], using the 2.5 MV Van de Graaff accelerator at Institut für Kernphysik of the University of Frankfurt, noted a 4.5σ deviation from expectation in the angular distribution of e^+e^- from Internal Pair Conversion (IPC) of the ^8Be M1 resonance. Analysis and Simulations of the signal that was seen led to the conclusion that a neutral boson of mass 9 MeV was a possible explanation that could not be ruled out by existing constraints [17, 18].

A 2015 experiment at the ATOMKI 5 MV Van de Graaff accelerator sought to repeat this measurement to further study the reported anomaly [19]. This experiment again saw an excess of e^+e^- pairs beyond the expectation of IPC. A subsequent analysis of these results has shown that the 6.8σ anomaly is consistent with a new particle with a mass of 16.84 MeV, dubbed X17. A followup experiment by the ATOMKI group was conducted on the 20.01 MeV $0^- \rightarrow 0^+$ transition in ^4He . The 2019 preprint of these results reports an e^+e^- excess consistent with the so-called X17 particle [20].

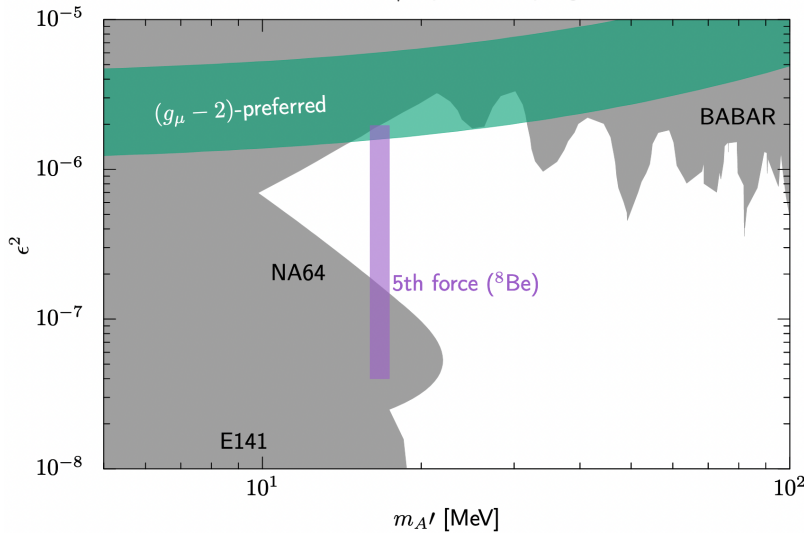


Figure 4: Current constraints on a fifth force explanation of the ^8Be anomaly. The vertical axis is the leptonic coupling strength relative to α_{QED} , with horizontal axis the mass of the mediator. Excluded regions, in gray, are taken from measurements that depend solely on leptonic interactions. Dark photon exclusions via hadronic measurements are not shown. Reproduced from Ref. [21].

Feng *et al.* [8] analyzed this signal against existing constraints. The proposed explanation is that the signal is from the decay of a protophobic gauge boson that mediates a fifth force with a length scale of 12 fm. This explanation can also possibly explain the muon anomalous magnetic

moment and an excess of $\pi^0 \rightarrow e^+e^-$ decays. The current constraints from leptonic production mechanisms, where the effective coupling to a new force-carrier is proportional to electric charge, are shown in Fig. 4. For more generic fifth-force models with quark flavor-dependent couplings [8], a much wider parameter space with multiple couplings must be considered.

The fifth force based explanations are being challenged by recent reanalyses [22] and the observed discrepancies could be the result of as-yet-unidentified nuclear reactions or experimental effects. Nonetheless, these results have garnered a lot of attention, and must be independently validated with the highest urgency.

3.4 Current Constraints

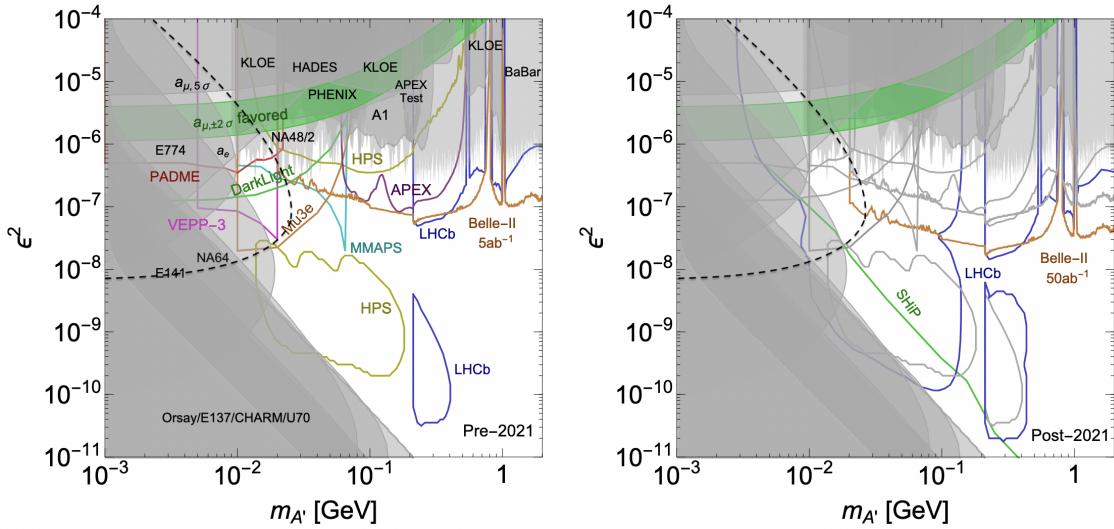


Figure 5: Sensitivity to X (sometimes called A') for exclusive experiments seeking visible decay modes $X \rightarrow l^+l^-$. Left: Experiments capable of delivering results soon. Shaded regions show existing bounds. Colored regions are experiments that are being prepared or are currently underway. The green band shows 2σ region in which an X can explain the discrepancy between the calculated and measured value for the muon ($g - 2$). The black dashed line is the exclusion from the recently reported NA64 experiment. Right: Longer term prospects beyond 2021 for experimental sensitivity. All projections on left plot are repeated in gray here. Reproduced from Ref. [1].

There are many constraints from previous experiments on the parameter space for a dark photon as shown in Fig. 5 reproduced from Ref. [1]. The parameter space of mass m_X and the square of the coupling ϵ^2 has been constrained from two sides by existing data. The low mass and small- ϵ^2 parameter space has been excluded primarily by previous beam-dump experiments [23, 24, 25] and the energy loss in supernovas from observations of the neutrinos they generate [26]. The constraints from the 2020 results of the NA64 experiment measuring e^+e^- decays [27] have been added to Fig. 5 as the black dashed line. In the NA64 experiment 8.4×10^{10} 150 GeV electrons were incident on a $\approx 30 - 40$ (depending on the run) radiation length (r.l.) active target-tungsten-calorimeter. The active target also served as a dump for the recoil electrons as well as the secondary particles emitted by the electron beam before the production of X . The subsequent decay of X

to e^+e^- would appear as a bump in the spectrum of events producing two showers, one in the active target and another one in a second downstream calorimeter, with the total energy of the two showers almost equal to the beam energy. The experiment described in this proposal has a radically different design with $\sim 2.7 \times 10^{16}$ electrons incident on a 2.5×10^{-4} r.l. target and a high resolution calorimeter and tracking detectors that will individually detect all three particles in the final state making it a direct detection experiment. The systematic differences between the two methods are further discussed in Sec. 9.

The larger- ϵ^2 values (10^{-6} - 10^{-4}) are excluded for a broad range of masses by searches at B-factories [28] and lepton $g - 2$ measurements [29]. With these constraints, there still exists a hole in MeV-scale region with coupling constant, ϵ^2 in the range of $10^{-6} - 10^{-10}$. Several experimental efforts such as DarkLight [21], MMAPS [30] and Mu3e [31] are being prepared and several others such as the HPS [32] and APEX [33] experiments at JLab are currently underway to cover parts of this hole as described in Sec. 9 and shown in Fig. 5 (left). While this hole in the parameter space is small, it is a high-priority search window as explanations for the motivations described above can exist within this previously unsearched region. This hole opens up even more if one considers the possibility of a flavor-dependent coupling, as any constraints derived from proton or muon beams would then be irrelevant to an electron beam search. Based on region of parameter space that is still unexplored and at the same time having healthy overlaps with other searches, we have designed an experiment to search the 3 – 60 MeV mass range as described in the next section.

4 Experimental Method

This experiment will focus on the bremsstrahlung-like production of dark sector particles from the initial electron or the scattered electron (both shown in Fig.6), in the 3 – 60 MeV mass range. When searching for new particles, it is of the utmost importance to minimize backgrounds in order to prevent false “bumps” in the mass spectrum. The primary QED background in this experiment (see Fig 7) are from the radiative pair production which is an irreducible background and the Bethe-Heitler trident reactions which can be kinematically suppressed.

The cross section for bremsstrahlung-like production of an X can be estimated within the Weizsäcker-Williams approximation [7] giving a total production rate of $N_X \sim N_e CT \epsilon^2 \frac{m_e^2}{m_X^2}$, where N_e is the number of incident electrons, T is the target thickness, m_X is the mass of the produced X , and ϵ^2 is the square of the dimensionless coupling constant of the X to SM matter. For $T \ll 1$ and m_X in the range of this experiment, the factor $\mathcal{C} \sim 5$ (it is related to the effective photon flux, atomic screening, and nuclear size effects). This implies that the total X production rate is suppressed relative to photon bremsstrahlung by $\sim \epsilon^2 \frac{m_e^2}{m_X^2}$ [7]. Moreover, the bremsstrahlung produced X is sharply peaked at $y = \frac{E_X}{E_{beam}} \approx 1$, i.e. when an X is produced, it carries nearly the entire beam energy. Further, the emission of X is dominantly co-linear with the beam with a cut-off emission angle (θ_X) that is smaller than the opening angle of the decay products i.e. $\theta_X < m_X/E_{beam}$ [7]. In the limit of small m_X/yE_{beam} , the lab-frame opening angles θ_{\pm} and energies E_{\pm} of the X decay products are given by [7];

$$\tan(\theta_{\pm}) = \pm \frac{1}{\gamma} \sqrt{\frac{1 \mp \cos(\theta_{CM})}{1 \pm \cos(\theta_{CM})}} + \tan(\theta_X)$$

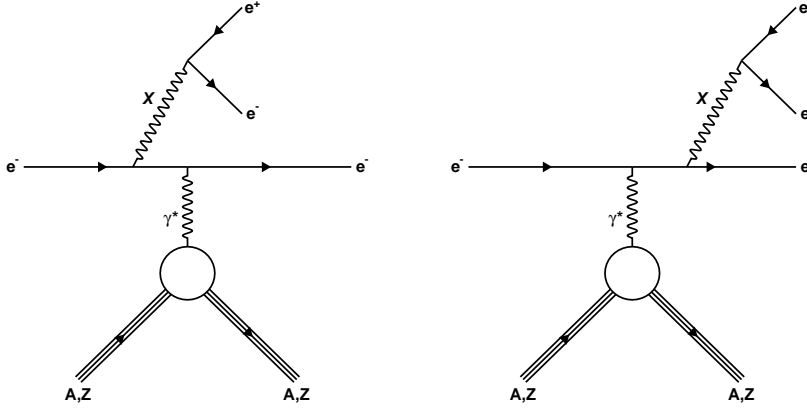


Figure 6: Bremsstrahlung-like production of a dark photon X from electron scattering. The left diagram shows production from the incoming electron and the right diagram shows production from the scattered electron.

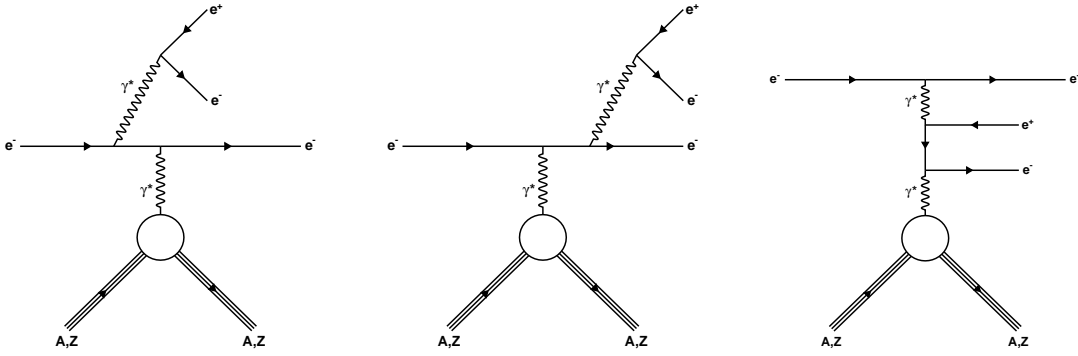


Figure 7: The QED background from radiative (left and middle) and Bethe-Heitler (right) process.

and

$$E_{\pm} = \frac{yE_{beam}}{2} (1 \pm \theta_{CM}),$$

where $\gamma = yE_{beam}/m_X$ and θ_{CM} is the the emission angle of the forward decay product relative to the direction of X in its rest frame. At the mass range probed in this experiment the recoiling electron largely balances the recoil of the X and the energy E_R and the angle θ_R of the recoiling electron in the laboratory frame are given by [7] ;

$$E_R = (1 - y)E_{beam} \approx m_X$$

and

$$\tan(\theta_R) \approx \sqrt{\frac{m_X}{E_{beam}}} \left(1 + \frac{m_X}{2E_{beam}} + \dots \right),$$

indicating the relatively wide angle of the recoiling electron relative to the X decay products. These kinematics characteristics of X production can be used to suppress the background from the

Bethe-Heitler trident reaction which can otherwise be prohibitively large. Once again using the Weizsäcker-Williams approximation it is found that Bethe-Heitler production is peaked at small y , it has $\cos(\theta_{CM}) \rightarrow 1$ and it is co-linear to the photon. Therefore, the kinematic characteristics of the Bethe-Heitler production is quite different from the signal (from X production) and from radiative backgrounds, which are peaked at large values of y and vary slowly with $\cos(\theta_{CM})$. This implies that requiring $y > 1 - \delta$, with δ near or below its median value $\bar{\delta} = \max(m_X/E_{beam}, m_e/m_X)$, keeps a large fraction of the signal while suppressing the Bethe-Heitler background by a factor of δ . Similarly, since the signal from X production is relatively flat in $\cos(\theta_{CM})$ the Bethe-Heitler background can be suppressed by constraining the cosine of the opening angles of the two decay products to be near unity [7].

The proposed experiment will use a “bump hunt” technique in the direct detection search of heretofore unknown MeV mass particles. The experiment is designed based on the kinematic constraints described above. A 2.2 and 3.3 GeV CW electron beam from CEBAF will be incident on a retractable ultra-thin target consisting of a 1 μm Tantalum foil. The scattered particles will traverse the 7.5 m long flight path in a vacuum chamber consisting of the PRad target chamber and the PRad vacuum chamber on-route to a pair of common ionization volume GEM chambers coupled to the HyCal EM calorimeter. All 3 cluster events with the sum of total energy deposited in the calorimeter that satisfies the condition $E_{sum} > 0.7 \times E_{beam}$ will be recorded and searched for “bumps” in the the $M_{e^+e^-}$ invariant mass spectrum reconstructed from these events. The tracking provided by the pair of GEM chambers will be used to suppress background events from the large area window at the exit of the vacuum chamber. The GEM chambers will also be used to veto the neutral particles. Only the PbWO_4 part of the HyCal calorimeter will be used in the experiment. The lower resolution of the lead-glass part makes it unusable in this experiment. The experimental method discussed here applies directly to any spin-1 boson in the dark sector that decay directly to a lepton pair. The experiment is designed with several key features to provide a clean signal of any unknown particles that may exist in the 3 – 60 MeV/ c^2 mass range:

- The experiment will detect the scattered electron along with the decay products of the dark photon (all three final states are detected - i.e. it is a direct detection experiment)
 - The full energy of the event can be reconstructed, reducing kinematic mimicking
 - It can be verified that the dark photon and the recoil electron are co-planar
- With the use of two GEMs spaced 10 cm apart, charged decays and recoil electrons can be tracked to ensure that they do not originate from the vacuum chamber exit window. The GEM detectors also help suppress the neutral background.
- The use of two beam energies (2.2 GeV and 3.3 GeV) will ensure that any background processes that mimic a bump can be identified

This optimized design can be implemented with the PRad setup with very minor modifications, making it a ready-to-run and uniquely cost-effective search for dark matter mediators in the 3 - 60 MeV mass range.

5 Experimental Setup

The proposed experiment plans to reuse the PRad setup (shown in Fig. 8) but with a Tantalum foil target placed 7.5 m upstream of the calorimeter. Only the high resolution PbWO_4 crystal part of the electromagnetic calorimeter will be used together with a new fADC based readout system for the calorimeter. Just as in the PRad experiment, the scattered electrons will travel through the 5 m long vacuum chamber with a thin window to minimize multiple scattering and backgrounds. The vacuum chamber matches the geometrical acceptance of the calorimeter. An extension piece will be added to the upstream end to couple the PRad target chamber to the super-harp which will now hold the target foil. A reducer ring will be attached to the downstream exit of the PRad vacuum chamber and a new 1 mm thick Al exit window will be used such that it matches the PbWO_4 portion of the calorimeter. Two layers of GEM detectors will add a modest tracking capability to help reduce the photon background and to reduce the background originating from the vacuum chamber exit window.

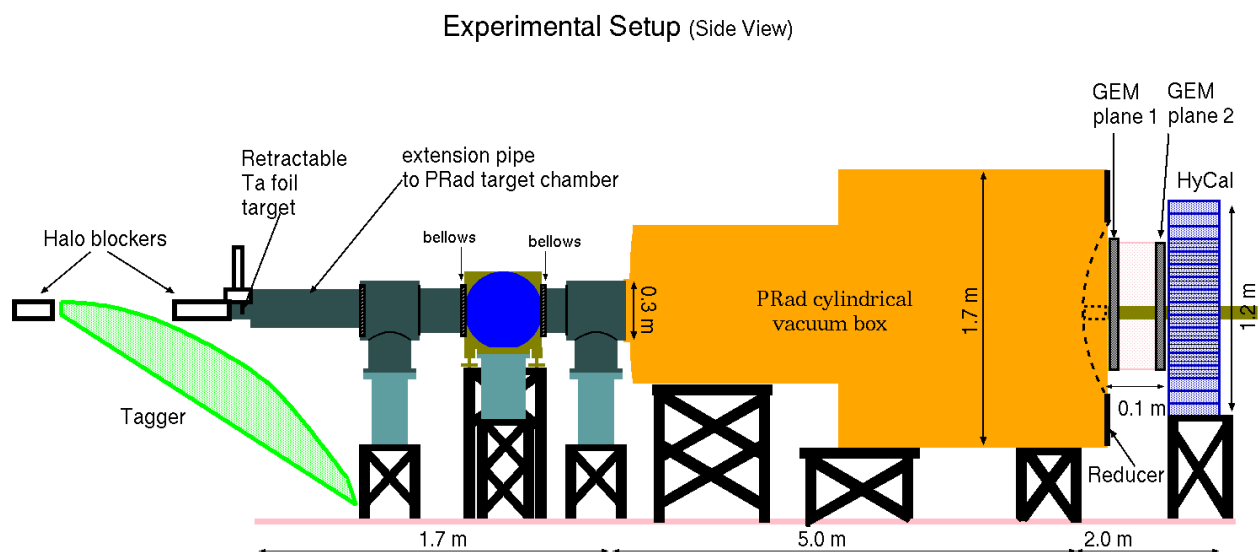


Figure 8: Schematic of the experimental setup.

The elements of the experimental apparatus along the beamline are as follows:

- Ta foil target held inside the super-harp enclosure.
- The PRad target chamber attached to the super-harp via an extension piece and coupled to the two stage, large area vacuum chamber with a single thin 1-mm Al. window at the calorimeter end
- A pair of GEM detector planes, separated by about 10 cm for coordinate measurement as well as tracking.
- High resolution PbWO_4 crystal calorimeter (the Pb-glass part of the HyCal will not be used) with a fADC based readout.

5.1 Electron beam

Table 1: Beam parameters for the proposed experiment

Energy (GeV)	current (nA)	polarization (%)	size (mm)	position stability (mm)	beam halo
2.2	50	Non	< 0.1	≤ 0.1	$\sim 10^{-6}$
3.3	100	Non	< 0.1	≤ 0.1	$\sim 10^{-6}$

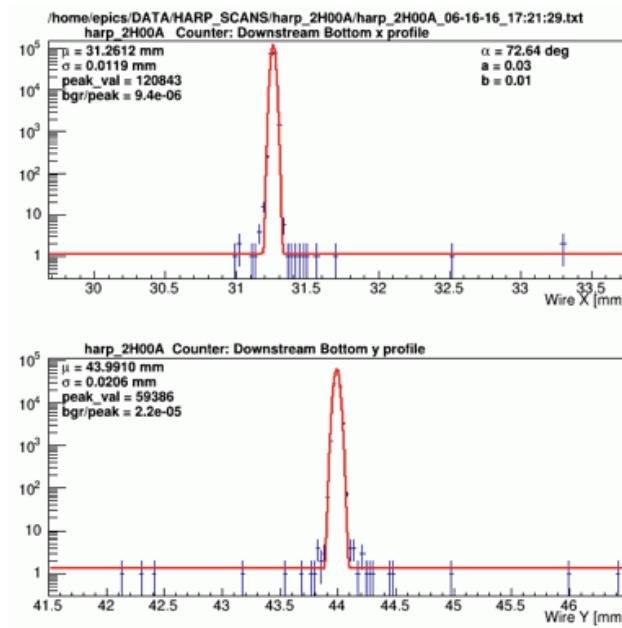


Figure 9: Typical beam profile during the PRad experiment, showing a beam size of $\sigma_x = 0.01$ mm and $\sigma_y = 0.02$ mm.

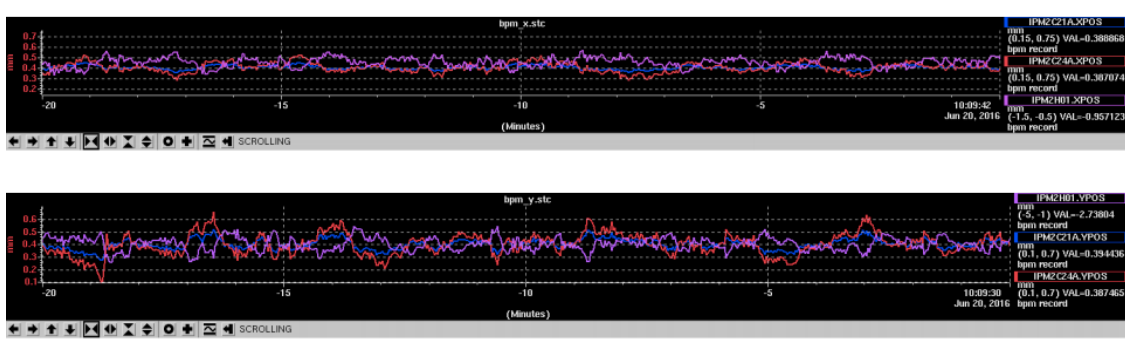


Figure 10: Beam X,Y position stability ($\simeq \pm 0.1$ mm) during the PRad experiment.

We propose to use the CEBAF beam at two incident beam energies $E_0 = 2.2$ and 3.3 GeV for this experiment. The beam requirements are listed in Table 1. All of these requirements or

even better were achieved during the PRad experiment. A typical beam profile during the PRad experiment is shown in Fig. 9 and the beam X, Y position stability was $\simeq \pm 0.1$ mm as shown in Fig. 10.

5.2 Target

Table 2: Material properties

Material	Z	Melting Point (°C)	Density (g/cc)	Tensile strength (1000 psi)	Min. foil thickness μ m
Ta	73	2996	16.6	35-75	0.5
W	74	3410	19.3	100-500	2.5

A $1 \mu\text{m}$ thin Ta foil (2.5×10^{-4} r.l.) target will be placed inside the super-harp setup that is part of the PRad setup in Hall-B. The super-harp will be located right after the second beam halo blocker placed right after the Hall-B tagger in the Hall-B beamline. The target foil will be placed on the same ladder that holds the super-harp wires. The mechanism used to insert the super-harp wires into the electron beam will be utilized to insert or retract the target foil into and out of the beam. Tantalum was chosen because foils as thin as $0.5 \mu\text{m}$ are available commercially. Properties of Ta and W are compared in Table 2.



Figure 11: A photograph of the ~ 5 m long, two stage vacuum chamber used during the PRad experiment.

5.3 Large volume vacuum chamber

For the PRad experiment a new large ~ 5 m long, two stage vacuum chamber was designed and built. A photograph of the vacuum chamber is shown in Fig. 11. We will reuse this vacuum

chamber with a new reducer flange such that a single 1.0 m diameter, 37 mil thick Al. window at the downstream end of the vacuum chamber, just before the GEM detector, can be used. Thinner window material will also be explored. A photograph of the current 1.7 m diameter 2 mm thick window is shown in Fig. 12 (left) along with a sketch of the reducer flange (right) which will allow a smaller thinner window to be used for this proposed experiment. A 2-inch diameter beam pipe will be attached using a compression fitting to the center of the thin window. This vacuum chamber along with the PRad target chamber (without the target cell) and a new extension piece connecting it to the super-harp will ensure that the electron beam does not encounter any additional material other than the target foil, all the way down to the Hall-B beam dump. The vacuum chamber will also help minimize multiple scattering of the charged particles en route to the detectors.

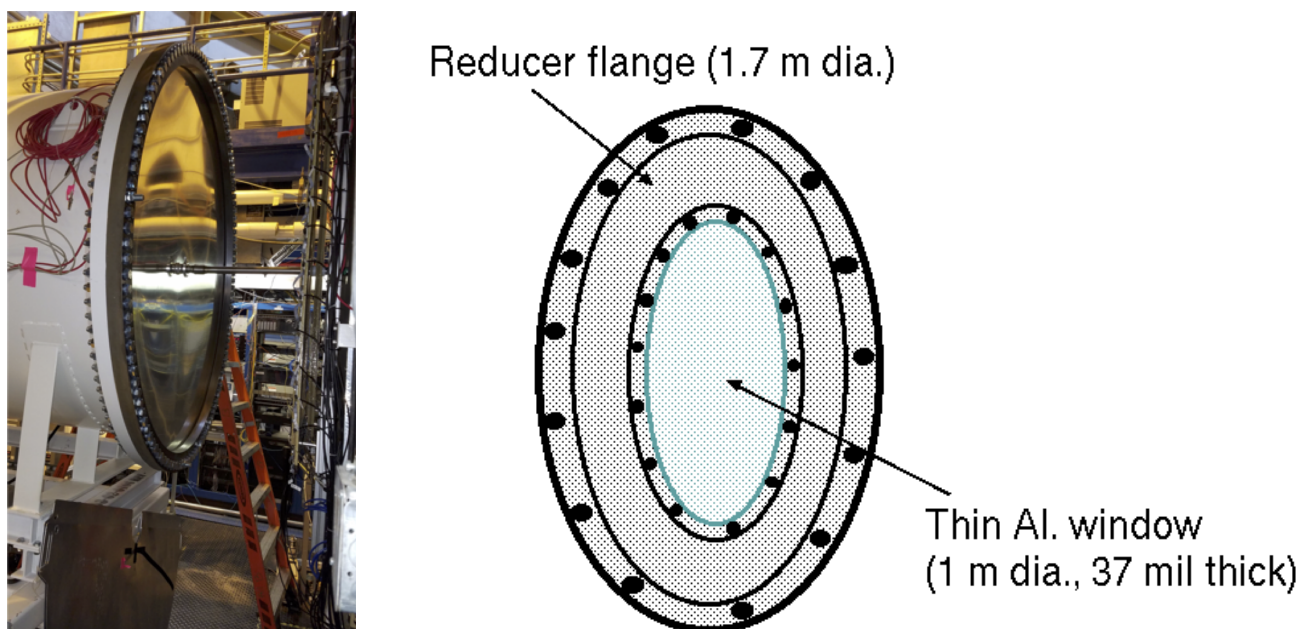


Figure 12: A photograph of the 1.7 m diameter thin window at one end of the vacuum chamber (left). A sketch of the reducer flange and 1.0 m diameter, 37 mil thick Al. window (right).

5.4 High resolution forward calorimeter

The scattered electrons and electron-positron pair in this precision experiment will be detected with a high resolution and high efficiency electromagnetic calorimeter. In the past decade, lead tungstate (PbWO_4) has become a popular inorganic scintillator material for precision compact electromagnetic calorimetry in high and medium energy physics experiments (*e.g.* CMS and ALICE at the LHC) because of its fast decay time, high density and high radiation hardness. The performance characteristics of the PbWO_4 crystals are well known mostly for high energies (>10 GeV) [34] and at energies below one GeV [35]. The PrimEx Collaboration at Jefferson Lab constructed a novel state-of-the-art multi-channel electromagnetic hybrid (PbWO_4 -lead glass) calorimeter (HyCal) [36] to perform a high precision (1.5%) measurement of the neutral pion lifetime via the Primakoff effect. The advantages of using the HyCal calorimeter was also demonstrated in the PRad experiment.

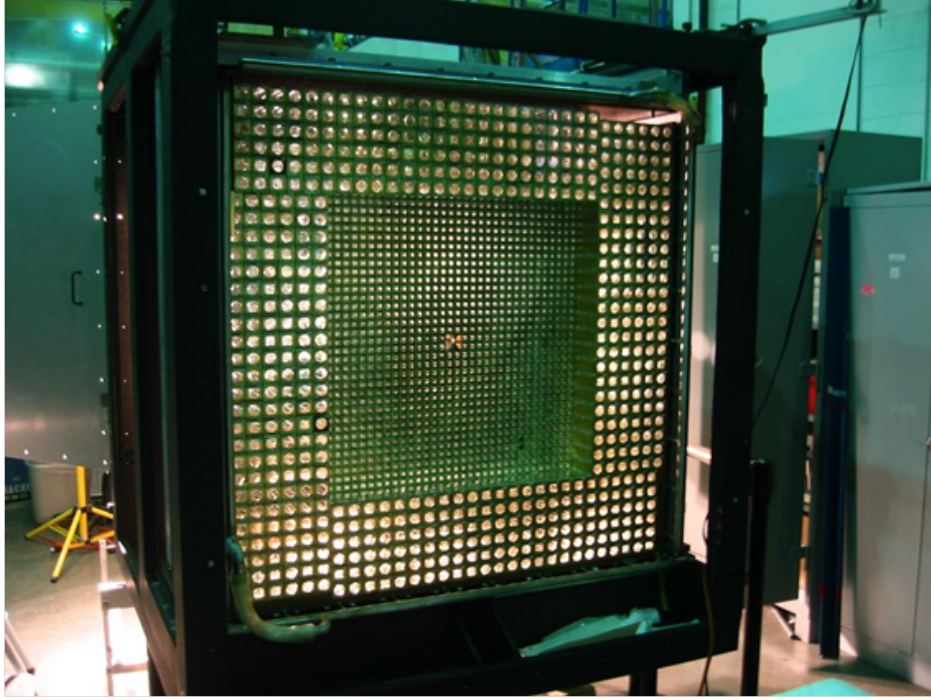


Figure 13: The PrimEx HyCal calorimeter with all modules of the high performance PbWO_4 crystals in place before installation of the light monitoring system.

For this experiment we are proposing to use only the PbWO_4 part of the calorimeter. A single PbWO_4 module is $2.05 \times 2.05 \text{ cm}^2$ in cross sectional area and 18.0 cm in length ($20X_0$). The calorimeter consists of 1152 modules arranged in a 34×34 square matrix ($70 \times 70 \text{ cm}^2$ in size) with four crystal detectors removed from the central part ($4.1 \times 4.1 \text{ cm}^2$ in size) for passage of the incident electron beam. As the light yield of the crystal is highly temperature dependent ($\sim 2\%/^\circ\text{C}$ at room temperature), a special frame was developed and constructed to maintain constant temperature inside of the calorimeter with a high temperature stability ($\pm 0.1^\circ\text{C}$) during the experiments. Figure 13 shows the assembled PrimEx HyCal calorimeter that was used in the PRad experiment. For this experiment the calorimeter will be placed at a distance of about 5.5 m from the target just as in PRad.

During PrimEx the energy calibration of HyCal was performed by continuously irradiating the calorimeter with the Hall B tagged photon beam at low intensity ($< 100 \text{ pA}$). An excellent energy resolution of $\sigma_E/E = 2.6\%/\sqrt{E}$ has been achieved by using a Gaussian fit of the line-shape obtained from the 6×6 array. The impact coordinates of the electrons and photons incident on the crystal array were determined from the energy deposition of the electromagnetic shower in several neighboring counters. Taking into account the photon beam spot size at the calorimeter ($\sigma=3.0 \text{ mm}$), the overall position resolution reached was $\sigma_{x,y} = 2.5 \text{ mm}/\sqrt{E}$ for the crystal part of the calorimeter. The calorimeter performed as designed during the experiment, as shown in Figs. 14-16, which shows the resolution achieved during the PrimEx experiment and the linearity of the detector response.

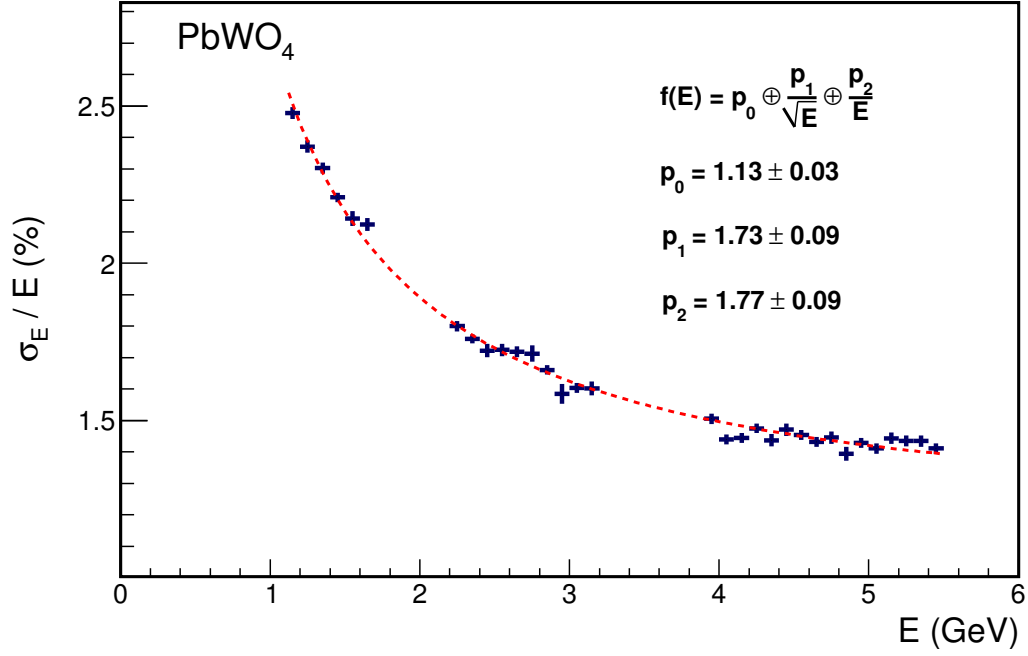


Figure 14: Energy resolution of the PbWO₄ crystal part of the HyCal calorimeter. These data are from the PrimEx experiment.

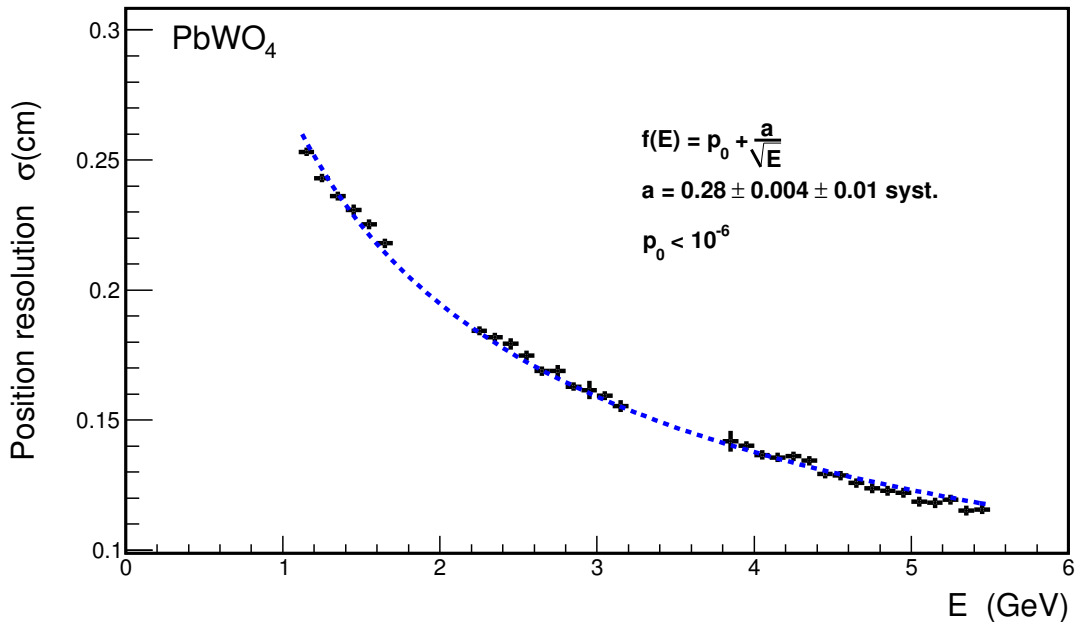


Figure 15: Position resolution of the PbWO₄ crystal part of the HyCal calorimeter. These data are from the PrimEx experiment.

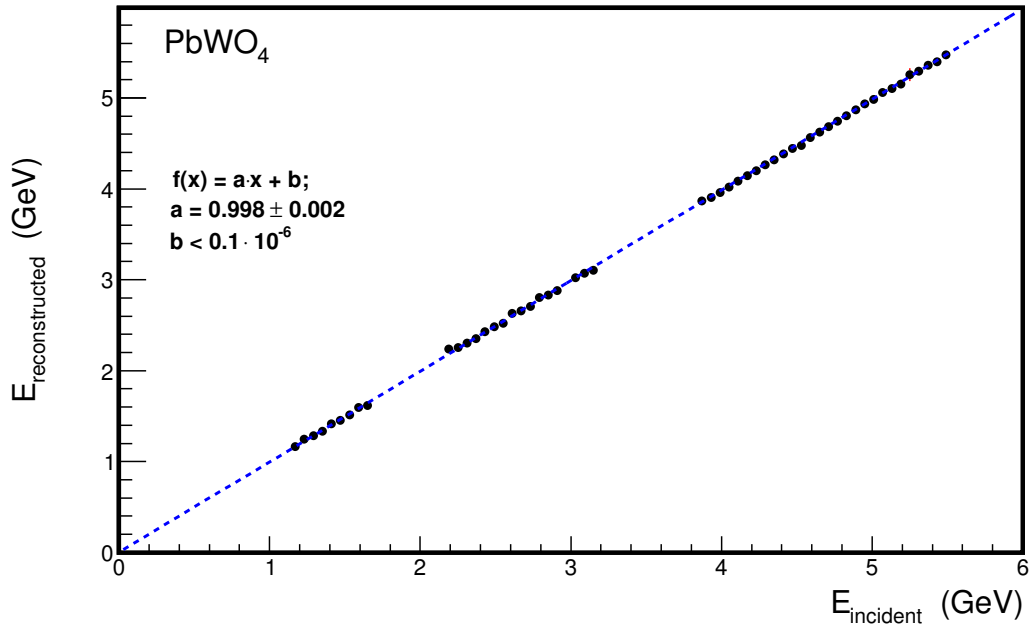


Figure 16: The linearity of the detector response for the PbWO₄ crystal part of the HyCal calorimeter. These data are from the PrimEx experiment.

5.5 GEM based coordinate detectors



Figure 17: The PRad GEM chambers (left) and the GEM chambers mounted on the HyCal during the experiment (right).

Two planes of 1.0 m×1.0 m GEM detector layers separated by 10 cm wide helium volume will be built by the UVa group for this experiment. These GEM detector layers will be similar in their basic design to the GEM layer used in the PRad experiment; however, as described below, the GEM detectors for this experiment will be optimized to reduce the material thickness compared to

the PRad GEMs. The GEM detectors have been shown to achieve $\sim 70 \mu\text{m}$ resolution in the PRad experiment. Similar to the PRad experiment, a custom designed through hole with a 4 cm radius will be built into GEM detectors at the center of the active area for the passage of the beam-line. The 10 cm thick helium box between the two GEMs will be built with no front and back windows. The two GEMs will be mounted on the front and the back completing the helium volume. The hole for the beam-line will continue through a pipe in the helium box. The chamber-tracker box will be mounted to the front face of the HyCal calorimeter using a custom mounting frame.

The material thickness of the two GEMs will be reduced using the following approaches.

- Each GEM will be assembled as a double GEM detector with two GEM foils, as opposed to a triple GEM detector. Double GEM detectors have been demonstrated to work successfully in the past.
- The GEMs will be operated using a helium based gas mixture as opposed to an Argon based gas mixture.
- We will build each GEM without using the honeycomb support layer underneath the bottom readout plane. In a standard GEM detector this support layer holds the slightly elevated pressure inside the detector against the atmosphere. However, in the setup proposed here, the readout layer of each GEM sits against the helium box volume which will be maintained at the same pressure as inside the GEMs. As such, the support layers could be eliminated in this case reducing the material thickness by over 0.2% r.l. A large area GEM prototype based on this principle was successfully built and beam tested by the UVa group as part of EIC detector R& D.

With these optimizations the material thickness of single GEM will be reduced to be about 0.3%, as opposed to about 0.6% for a standard GEM. With this, the total material thickness for the whole tracker including the two GEMs and the helium volume will be approximately 0.6%.

In addition to the above improvements, we will explore the possibility of building the GEMs using ultra-thin chromium GEM foils as opposed to standard copper GEM foils. A conventional GEM foil consists of an insulator made of a thin Kapton foil (about $50 \mu\text{m}$) sandwiched between two layers of copper (each about $5 \mu\text{m}$ thick). The new chromium GEM foils, recently developed at the CERN GEM workshop, have the copper layers of the foil removed, leaving only a $0.2 \mu\text{m}$ layer of Chromium on either side of the Kapton. The material thickness of a GEM module made of Copper-less foils is about 0.2% radiation lengths. The UVa group has fabricated and successfully operated chromium GEM detectors in beam test runs at Fermilab.

The GEM detectors will have 2D x-y strip readout. The readout of the two GEM layers requires approximately 15 k electronic channels. This readout for the proposed experiment will be done by using the high-bandwidth optical link based MPD readout system recently developed for the SBS program in Hall A. This system is currently under rigorous testing. This new system uses the APV-25 chip used in the PRad GEM readout. However, the readout of the digitized data is performed over a high-bandwidth optical link to a Virtual Trigger Processor (VTP) unit in a CODA DAQ setup.

Using the GEM layers for tracking the events originating from the target can be distinguished from those originating from the vacuum chamber exit window as shown in Fig. 18.

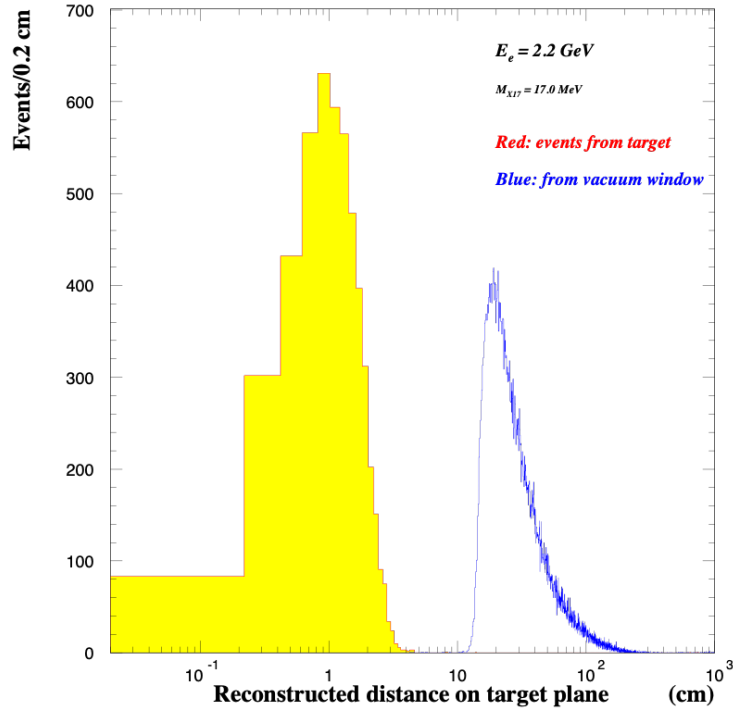


Figure 18: Events originating from the target and the events originating at the vacuum chamber exit window as reconstructed using tracking information from the GEM detectors.

5.6 Electronics, data acquisition, and trigger

The high resolution calorimeter in this proposed experiment will have around 1152 channels of charge and timing information. These will be readout using the JLab designed and built flash-ADC modules (FADC250), each with 16 channels. The DAQ system for the calorimeter is thus composed of 72 FADC250 modules that can be held in 5 16-slots VXS crates. The major advantages of the flash-ADC based readout are the simultaneous pedestal measurement (or full waveform in the data stream), sub-nanosecond timing resolution, fast readout speed, and the pipeline mode that allows more sophisticated triggering algorithms such as cluster finding.

Additionally, some VME scalers will be read out and periodically inserted into the data stream.

The DAQ system for the proposed experiment is the standard JLab CODA based system utilizing the JLab designed Trigger Supervisor. A big advantage of the CODA/Trigger Supervisor system is the ability to run in fully buffered mode. In this mode, events are buffered in the digitization modules themselves allowing the modules to be “live” while being readout. This significantly decreases the deadtime of the experiment. With the upgraded flash-ADC modules we expect to reach a data-taking rate of about 25 kHz events. Such a capability of the DAQ system has already been demonstrated by CLAS12 experiments.

A large fraction of the electronics needed for the DAQ and trigger, including the high voltage crates and all necessary cabling for the detectors, are available in Hall B from the PRad experiment.

The first level hardware trigger will be based on the total energy deposited being very close to the beam energy (> 300 MeV below the beam energy) while also meeting the DAQ rate require-

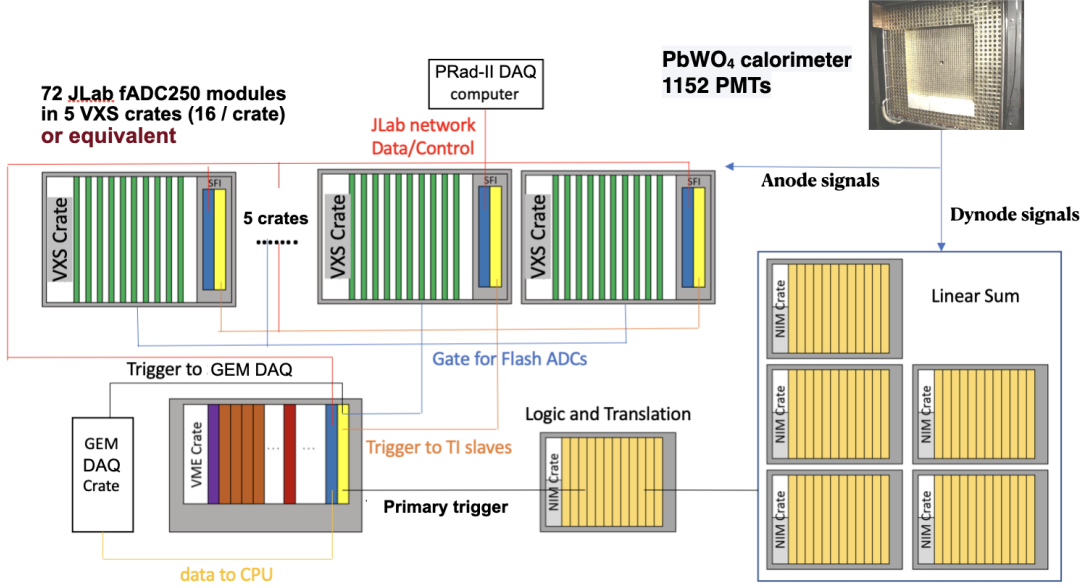


Figure 19: A modern FADC based DAQ will be used with the primary trigger formed using the sum of all dynode outputs from each of the crystals.

ments. The primary trigger will be formed from the PbWO₄ calorimeter by only using the analog sum of all dynode outputs from each of the crystal cells (see Fig. 19). The trigger condition will be that the total energy deposited in the PbWO₄ part of the calorimeter is larger than $0.7 \times E_{beam}$. We will collect all three cluster events that have cluster energy within $(0.02 - 0.85) \times E_{beam}$. The GEM detector will not be included in the trigger implying that all charged as well as neutral 3-cluster events will be recorded. A single crystal cluster separation resolution is assumed, as demonstrated in the PrimEx and PRad experiments.

5.7 Detection Efficiency and Resolutions

Fig. 20 shows the efficiency of detecting 3-cluster events in the PbWO₄ calorimeter with the scattered electron having energy between $(0.03 - 0.7) \times E_{beam}$ and detected along with the e^+e^- pair from the X decay for $E_{beam} = 2.2$ and 3.3 GeV. The two innermost layers of HyCal are excluded. It also includes the effect of displaced decay vertex on the geometrical acceptance (important only at the low mass and low e^2 range). This shows that the proposed experimental setup is sensitive to the 3 - 60 MeV mass range. At lower beam energies the detection efficiency has a steep fall-off with invariant mass. Although the 2.2 GeV detection efficiency is lower than the 3.3 GeV efficiency it will serve as a systematic check and will also be used to boost the combined statistical significance.

The invariant mass resolution for a hypothetical X particle with a mass of 5, 17 and 25 MeV is shown in Fig. 21 when using the calorimeter, GEM and vertex reconstruction with beam energy of 2.2 and 3.3 GeV is shown in Fig. 21. The impact of the vertex reconstruction with the HyCal and the two GEM planes is demonstrated in Fig. 22 (left) where the invariant mass resolution with (top) and without (bottom) the vertex reconstruction is shown for 2.2 GeV beam energy. As can

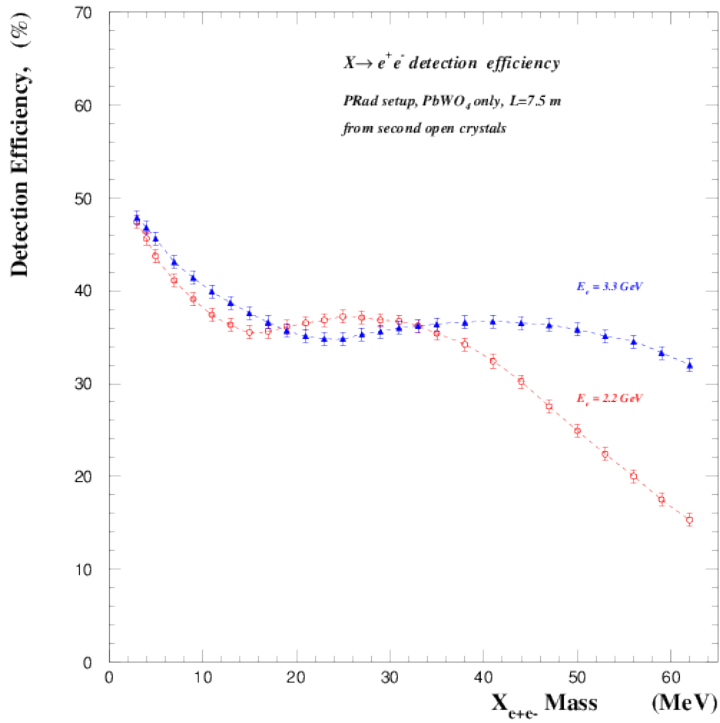


Figure 20: The efficiency of detecting the scattered electron with energy between $(0.03 - 0.7) \times E_{\text{beam}}$ along with the e^+e^- pair in the PbWO_4 calorimeter for $E_{\text{beam}} = 2.2$ and 3.3 GeV.

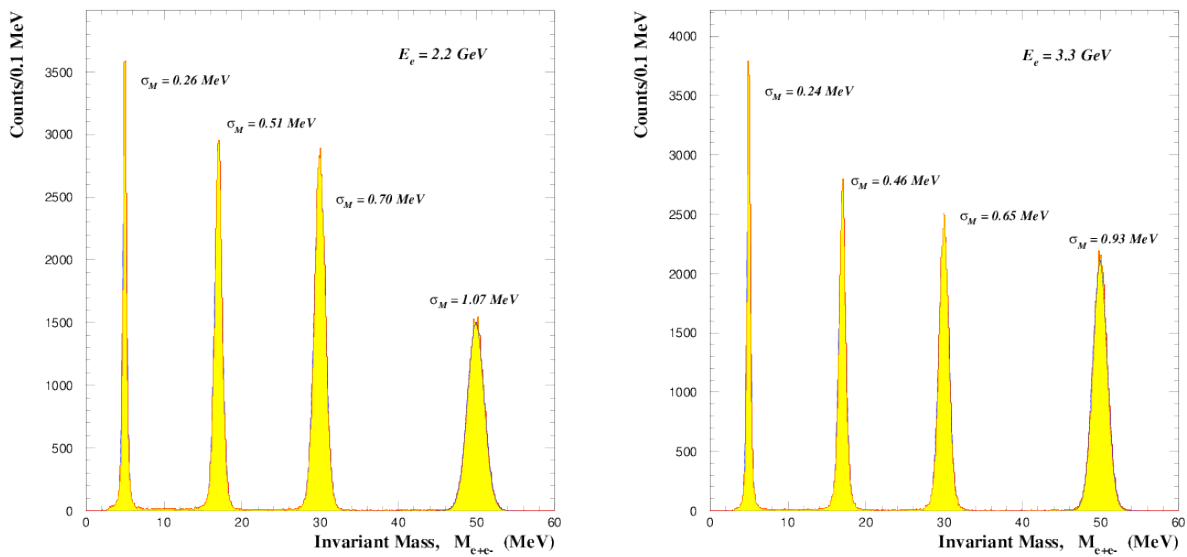


Figure 21: The e^+e^- invariant mass resolution at 2.2 GeV (left) and 3.3 GeV (right).

be seen in these plots, the invariant mass resolution is significantly improved when using the target vertex. Using the GEMs alone, however, will serve as an additional systematic check of our results. Events that originate in the target will have the same centroid for the reconstructed invariant mass using both methods. This will help to identify false peaks in our analysis. The azimuthal angle resolution is $\sim 0.9^\circ$ shown in Fig. 22 (right). This will help ensure the coplanarity of the X particle production.

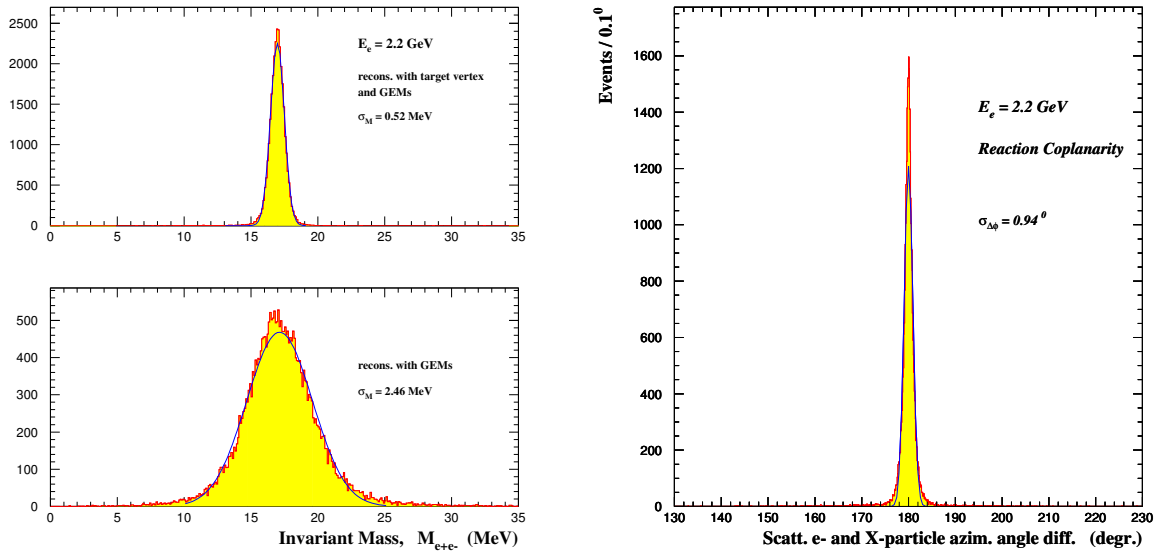


Figure 22: (left) The invariant mass resolution at 2.2 GeV with vertex reconstruction (top) and without vertex reconstruction (bottom). (right) The difference in azimuthal angle between scattered electron and X particle. The azimuthal angle resolution of $\sim 0.9^\circ$ will be used to ensure the coplanarity of the X particle production.

6 Monte Carlo Simulations of the Background

A comprehensive simulation of the experiment was carried out using the Geant simulation package developed for the PRad experiment. This simulation takes into account realistic geometry of the experimental setup, and detector resolutions. The generated scattering events were propagated within the Geant simulation package, which included the detector geometry and materials of the PRad setup. This enabled a proper accounting of the external Bremsstrahlung of particles passing through various materials along its path. The simulation included photon propagation and digitization of the simulated events. These steps are critical for the precise reconstruction of the position and energy of each event in the HyCal. The X production and decay into e^+e^- was according to the rate equation shown in Sec. 4 with the X produced along the virtual photon direction. The decay length was also taken into account. The simulated scattered electron spectrum as well as the energy spectrum of the e^+e^- decay of the X particle are shown in Fig. 23 for the 2.2 GeV beam energy.

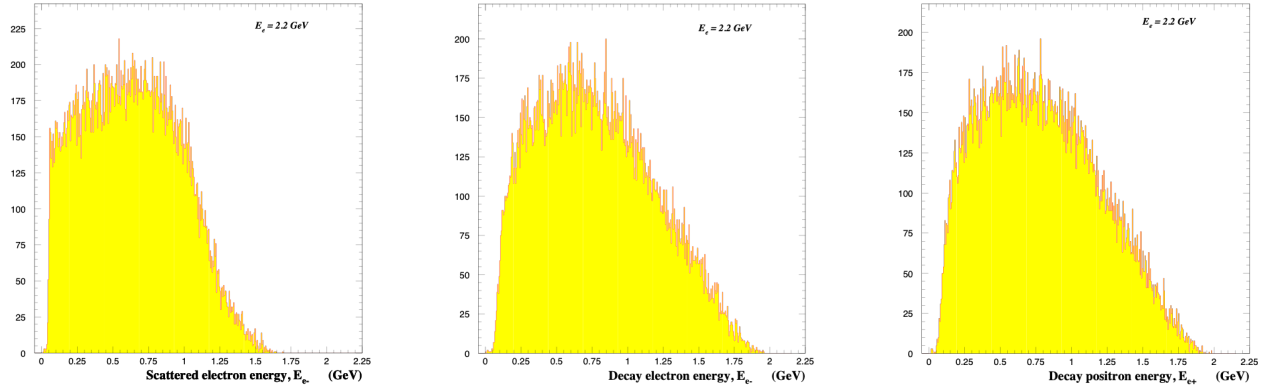


Figure 23: The simulated scattered electron energy spectrum (left) and the energy spectrum of the electron and positron from the decay of the X particle.

The ep elastic and $e - e$ Møller generators developed for the PRad experiments were used to verify that these background processes are kinematically suppressed. We have also simulated the Bethe-Heitler and the radiative background processes. The Bethe-Heitler background process is kinematically suppressed and the radiative process is the irreducible background. The background was simulated for about 3.5 sec of 3.3 GeV electron beam with a current of 100 nA (corresponding to 2.2×10^{12} electrons on target). The reconstructed invariant mass $M_{e^+e^-}$ spectrum for these simulated events are shown in Fig. 24 (left). Simulation of additional statistics is underway but meanwhile we have fit the simulated background to a sum of a Landau distribution and a constant distribution. The fit was used to scale the background by sampling the number of events bin-by-bin to give the expected background for 30 days of 3.3 GeV beam at 100 nA, as shown in Fig. 24 (right). The shape of the background can be validated by comparing it to the background using similar event selection of PRad data (see Fig. 32 in Appendix A).

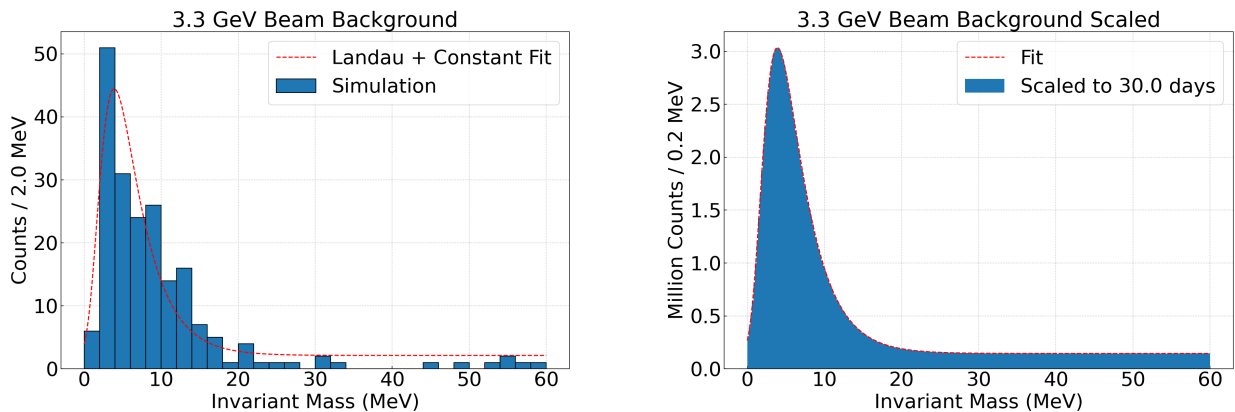


Figure 24: (left) The simulated background for 3.5 sec of 100 nA beam at 3.3 GeV (corresponding to 2.2×10^{12} electrons on target) and a fit to a sum of Landau + constant distribution. (right) The background counts are scaled to the beam time according to the fit, the number of events are sampled bin-by-bin.

7 Beam Time Request and Statistics

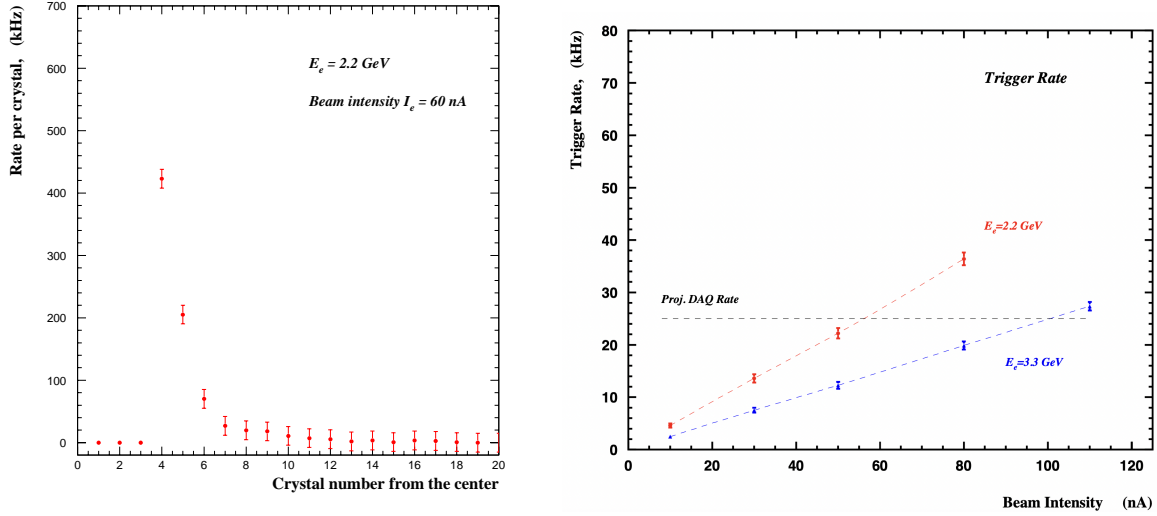


Figure 25: (left) The rate per crystal for 60 nA of electron beam at a 2.2 GeV beam energy. (right) The trigger rate vs beam current.

The trigger rate is calculated for a 2.2 GeV and 3.3 GeV electron beam incident on a $1 \mu\text{m}$ Ta target with the calorimeter placed 7.5 m from the target. We count starting from the 3rd inner most layer of crystals (2nd innermost crystal after the layer covered with a W absorber), with the condition that the total energy deposited in the PbWO_4 part of the calorimeter is larger than $0.7 \times E_{\text{beam}}$. We count all three cluster events that have cluster energy within $(0.02 - 0.85) \times E_{\text{beam}}$. Since the GEMs detectors are not used in the trigger all clusters, charged or neutral, are counted. The charged are $\sim 1\%$ of all 3 cluster events. A cluster separation resolution of one crystal is assumed as demonstrated in previous experiments that have used the HyCal calorimeter. The calculated rate per crystal for 60 nA of electron beam at 2.2 GeV beam energy is shown in Fig. 25 (left) and the trigger rate as a function of the beam current is shown in Fig. 25 (right). Given the projected maximum DAQ rate of 25 kHz we have used 50 nA beam current at 2.2 GeV and 100 nA beam current at 3.3 GeV to calculate the beam time. As shown in table 3, we request 20 days

Table 3: The beam time request

	Time [days]
Setup checkout, tests and calibration	4.0
Production at 2.2 GeV @ 50 nA	20.0
Production at 3.3 GeV @ 100 nA	30.0
Energy change	0.5
No target background sampling at 2.2 & 3.3 GeV	5.5
Total	60.0

at 50 nA for the 2.2 GeV beam energy and 30 days at 100 nA at 3.3 GeV and total of 5.5 days for background running without a target. An additional 4.0 days are requested for calibration of the calorimeter and 0.5 days for energy change for a total of 60 days of beam time.

8 Projected Results

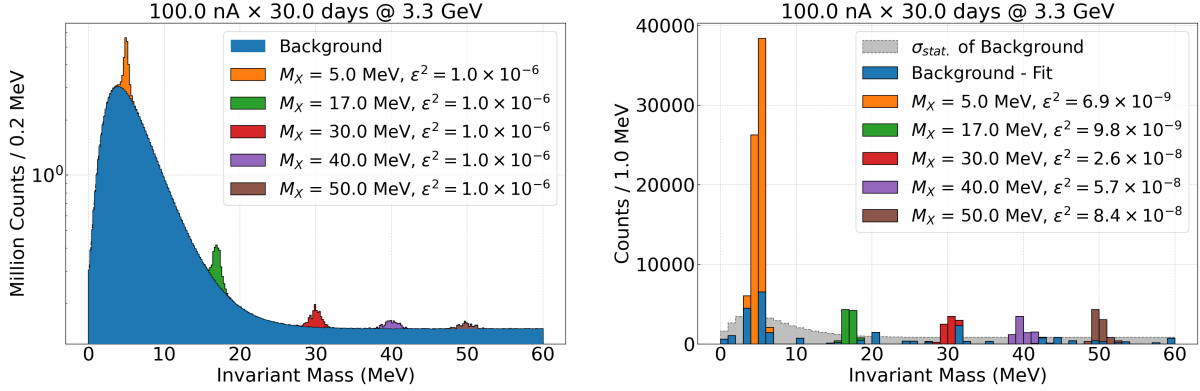


Figure 26: Projections of 30 days of beam time with 3.3 GeV beam energy and 100 nA beam current. (left) The distribution of signals and background with various m_X assuming $\epsilon^2 = 10^{-6}$ for illustration of the signal position and width. (right) The signal distribution over the background subtracted by fit, assuming ϵ^2 at the threshold to reach a 5.0 significance within $\pm 3\sigma$ of the signals.

The projected sensitivity to ϵ^2 is dominated by the 3.3 GeV run due to lower background level and better acceptance over the mass range of search. The projections for 30 days of 3.3 GeV beam at 100 nA are shown in Figure 26. The production rates for the X particle is calculated using the rate equation described in Sec. 4.

$$N_X = 5 \times N_e T \epsilon^2 \frac{m_e^2}{m_X^2},$$

where N_e is the number of incident electrons (2.2×10^{12} for 30 days at 100 nA), T is the target thickness (2.5×10^{-4} r.l.), m_X is the mass of the produced X , and ϵ^2 is the square of the dimensionless coupling constant of the X to SM matter. The decay length which leads to a displaced decay vertex was calculated as [7, 32],

$$l_{decay} = \gamma c \tau \approx \frac{3E_X}{\alpha m_X^2 \epsilon^2}.$$

The displaced decay vertex has an impact on the geometrical acceptance at the lowest mass and lowest ϵ^2 ranges covered in this proposed experiment. As designed this proposal does not have sufficient vertex resolution to measure the displaced decay vertex. However, a displaced vertex type experiment could be designed with additional tracking.

The lowest ϵ^2 that can be reached is calculated for $m_X = 5, 17, 30, 40,$ and 50 MeV, using

$$\frac{N_{\text{signal}}}{\sqrt{N_{\text{signal}} + N_{\text{bgd}}}} \geq 5,$$

incorporating simulated detection efficiencies. The background counts within $\pm 3\sigma_{m_X}$ mass range was calculated from the scaled simulated background for each of the 3 test m_X values. For masses ≤ 10 MeV the impact of the displaced vertex on the detection efficiency determines the lowest ϵ^2

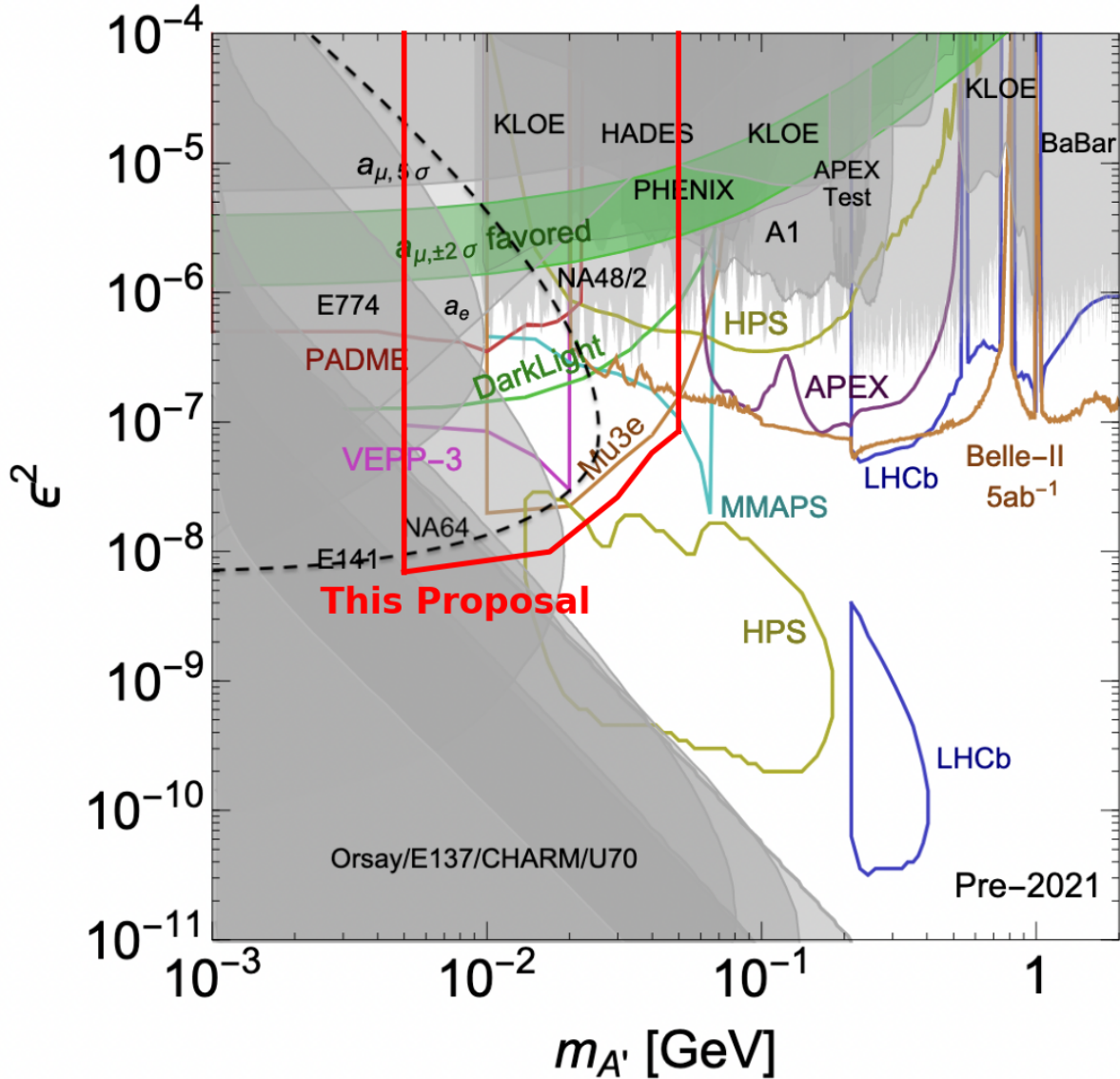


Figure 27: Projected coverage of the square of the coupling constant (ϵ^2) and mass (m_X) parameter space by this proposed experiment is shown as the thick red lines for the combined statistics of the two beam energies. The projections are superimposed on top of the constraints plot shown in Fig. 5 which was adapted from Ref. [1].

achievable. The projected mass resolutions, background counts, signal and the sensitivity for each of the m_X values is listed in Table 4. 2.2 GeV runs will serve as reference runs to better understand the background and the signal, so it was conservatively estimated that 50% of their statistics can be combined into the 3.3 GeV data for the final results. Using these range of sensitivities the bounds for the $\epsilon^2 - m_X$ parameter space is plotting in Fig. 27 for the combined projected statistics.

Table 4: Search Sensitivity

m_X MeV	σ_{m_X} MeV	Background Counts	Signal Counts (5.0 Significance)	Lowest ϵ^2	lowest ϵ^2
30 days of 3.3 GeV at 100 nA					combined with signal from 20 days at 2.2 GeV
5.0	0.263	22.02M	23.48k	6.86E-09	5.94E-09
17.0	0.467	3.60M	9.50k	9.83E-09	8.51E-09
30.0	0.692	3.06M	8.76k	2.60E-08	2.25E-08
40.0	0.938	4.08M	10.11k	5.71E-08	4.94E-08
50.0	1.009	4.38M	10.48k	8.37E-08	7.24E-08

9 Relationship to Other Experiments

As described in Sec. 3, there are a number of motivators to search for hidden sector particles on the MeV scale. As such, there are a number of other experiments with physics goals related to this proposal. At Jefferson Lab, there are several experiments both approved and proposed to search for hidden sector particles: APEX, HPS, and DarkLight. At other laboratories, there is NA64 and MAGIX.

APEX

The A' Experiment (APEX) experiment will run in Hall A at JLab. The experiment uses a tungsten multi-foil target with an incident electron beam with a goal of producing a vector boson A' through a bremsstrahlung-like process. Using the two High-Resolution Spectrometers (HRSs), the e^+e^- decay of the A' will be detected. APEX will be sensitive to A' masses from 65 – 525 MeV with a coupling constant as small as $\epsilon^2 > 9 \times 10^{-8}$ [33]. The proposed experiment will complement the APEX experiment by searching lower masses and by being sensitive to neutral decay channels.

HPS

The Heavy Photon Search (HPS) is a search experiment that has began running and continues to run in Hall B at JLab. HPS uses a tungsten target with an incident electron beam with a goal of producing a vector boson A' through a bremsstrahlung-like process. A magnetic spectrometer setup downstream of the CLAS detector setup will detect any charged A' decay products and reconstruct the displacement of the vertex. HPS will be sensitive to A' masses from 20 – 1000 MeV with coupling constant as small as $\epsilon^2 > 10^{-7}$ from the resonance search and $10^{-8} \leq \epsilon^2 \leq 10^{-10}$ from the displaced vertex search [32]. The proposed experiment will reach lower masses and will

also have some overlap in the mass range (20 – 60 MeV). In the regions of overlap, this proposed experiment will complement the HPS program by partially filling in the coupling constant gap between the resonance and displaced vertex search methods. Using a magnetic spectrometer free setup, this proposal will also be sensitive to neutral decay channels of hidden sector particles.

DarkLight

DarkLight is a set of experiments at JLab to search for MeV-scale dark photons. An approved proposal from DarkLight focuses on a 100 MeV electron beam from the JLab energy recovery linac incident on a windowless hydrogen target. The DarkLight setup uses a 0.5 Tesla solenoid and silicon and gas tracking detectors to detect the e^+e^- decay of A' vector bosons in the 10 – 90 MeV mass range produced through a bremsstrahlung-like process. The DarkLight experiment will also be susceptible to the invisible decay of the produced A' [37, 38]. A more recent DarkLight proposal focuses on a 45 MeV beam from the CEBAF injector impinging on a Tantalum target. Two dipole spectrometers will measure the e^+e^- decay of an A' produced through a bremsstrahlung-like process. The magnetic spectrometers will be set to focus on the 17 MeV region to quickly reach a $\epsilon^2 > 3 \times 10^{-7}$ to test the X17 explanation of the ATOMKI anomaly discussed in Sec. 3.3 [21]. This proposed experiment, in the regions of overlap (10 – 60 MeV), will reach lower coupling constants, ϵ^2 , and will be sensitive to the neutral decay of produced hidden sector particles in that mass range. By using the existing PRad setup this proposal is cost-effective and essentially ready to run if approved.

NA64

The NA64 experiment is an active target beam dump experiment at the CERN Super Proton Synchrotron. NA64 searches for the e^+e^- decay of an A' produced through a bremsstrahlung-like process by 150 GeV electrons that strike WCAL, a calorimeter comprised of tungsten and plastic scintillator that also functions as an active target. The most recent results exclude masses below about 25 MeV in the coupling constant range of $10^{-8} \leq \epsilon^2 \leq 10^{-6}$ [27]. An upgrade is planned that will close the coupling constant gap for the a mass of 17 MeV in an effort to test the X17 explanation of the ATOMKI anomaly [39]. While the exclusion from the 2020 NA64 results covers a large portion of the parameter space (3 – 60 MeV) that this proposed experiment will cover, there are some notably significant differences between the two approaches. The NA64 experiment had 8.4×10^{10} electrons incident on a $\approx 30 - 40$ (depending on the run) radiation length active target that served as a dump for recoil electrons and secondary particles produced by the beam. This proposed experiment will have 2.7×10^{16} electrons incident on a 2.5×10^{-4} radiation length target. Using a thinner target will mitigate multiple scattering of the beam and the X decay products. Moreover, the use of a high resolution calorimeter and additional tracking detectors will allow us to trigger on 3 cluster events. This allows for the detection of all three particles in the final state for the direct detection of the full kinematics of the X production. The suppression of the Bethe-Heitler background in this proposal is another major difference from the NA64 experiment. The NA64 experiment and this proposal have very different systematics and should be considered as complementary searches.

MAGIX

MAGIX is an experiment proposed to run at the MESA accelerator at Mainz. The experiment will use two magnetic spectrometers to study a varied physics program. One of the programs is to

detect the e^+e^- decay of a dark photon γ' produced through a bremsstrahlung-like process by 150 MeV electrons incident on a heavy nuclear supersonic gas jet target. The projected reach covers a mass range of about 8 – 70 MeV and will reach $\epsilon^2 > 8 \times 10^{-9}$ at low mass and $\epsilon^2 > 2 \times 10^{-7}$ at high mass[40, 41]. This proposal will cover a similar mass range as MAGIX (overlapping in 8 – 60 MeV) and reach smaller coupling constants, as well as being sensitive to neutral decay channels. Additionally, this proposal by using the existing PRad setup is essentially ready to run if approved.

10 Summary

We propose a direct detection search for hidden sector particles in the 3 – 60 MeV mass range using the magnetic-spectrometer-free PRad setup in Hall-B. This experiment will exploit the well-demonstrated PRad setup to perform a ready-to-run and cost-effective search. This search experiments is timely as well as urgent given the recent confirmation of the muon $(g - 2)$ anomaly and the 17-MeV particle proposed to account for the excess e^+e^- pairs found in a nuclear transition in ^8Be from one of its 1^+ resonance to its ground state, and the electromagnetically forbidden M0 transition in ^4He . In particular, the 3 – 60 MeV mass range remains relatively unexplored.

The experiment will use 2.2 GeV and 3.3 GeV CW electron beams, with a current of 50 – 100 nA, on a $1\mu\text{m}$ Ta foil placed in front of the PRad setup. All three final state particles will be detected in the PbWO_4 part of the HyCal calorimeter, and a pair of GEM chambers will be used to suppress the neutral background and the events not originating from the target. This technique will help effectively suppress the background from the radiative and Bethe-Heitler processes and provide a sensitivity of 7.2×10^{-8} - 5.9×10^{-9} to the kinetic mixing interaction coupling constant ϵ^2 . The experiment will help fill some of the void left by current, ongoing and other planned searches, thereby helping validate or place limits on hidden sector dark matter models. We request 60 days of beam time for this experiment.

Appendix A: Data Mining the PRad Experiment

This proposal will use the existing PRad setup with some small modifications. As such, we began the preparations for this experiment by analyzing the existing PRad data. PRad is an experiment in Hall B at JLab that aims to precisely measure the proton radius in order to solve the proton radius puzzle. The PRad experiment used a novel magnetic spectrometer-free design to measure $e - p$ elastic scattering at very low Q^2 and over a large Q^2 range simultaneously. The data was recorded at 1.1 GeV and 2.2 GeV and could kinematically be able to produce low MeV X candidates ($\approx 3 - 50$ MeV). As described in Sec. 4, the bremsstrahlung-like production of an X scales with atomic number Z^2 . The bulk of the data was taken with a windowless hydrogen gas target ($Z = 1$) which would have a very low X production rate and has the added complication of being an extended target. However, at each energy a short (1 hour) run was taken with a carbon foil target to better understand the associated systematics in the experiment [42]. This led us to look at the carbon foil data since it would have a 36 times higher cross section and avoids the complications associated with an extended target. As the production rate of an X in the PRad data would be very low, this search was intended to test the experimental methods of this proposal rather than a true attempt to find an X .

To begin, we selected events with exactly 3 clusters in the PbWO_4 part of HyCal that have matching hits in the GEM tracker, thus explicitly looking for an $X \rightarrow e^+e^-$ event and excluding other decay channels. Events which have extra clusters that do not match the event selection criteria are automatically vetoed. This setup does not have the ability to distinguish which clusters are the recoil electron and which would be the e^+e^- pair so all combinations are looped over, leading to three different pairings to reconstruct a potential X mass. Monte carlo simulations have shown that this looping procedure will still yield a clear peak in the event of a true X signal and that the incorrect pairings will create a smoothly distributed background. Figure 28 shows the invariant mass and energy conservation of events that pass these selection criteria. Figure 29 shows the difference of the beam energy and the sum of the energy of the three cluster. It is evident from these figures that the dominant event sources are inelastic. The bremsstrahlung-like production of an X is an elastic process, so these can easily be cut.

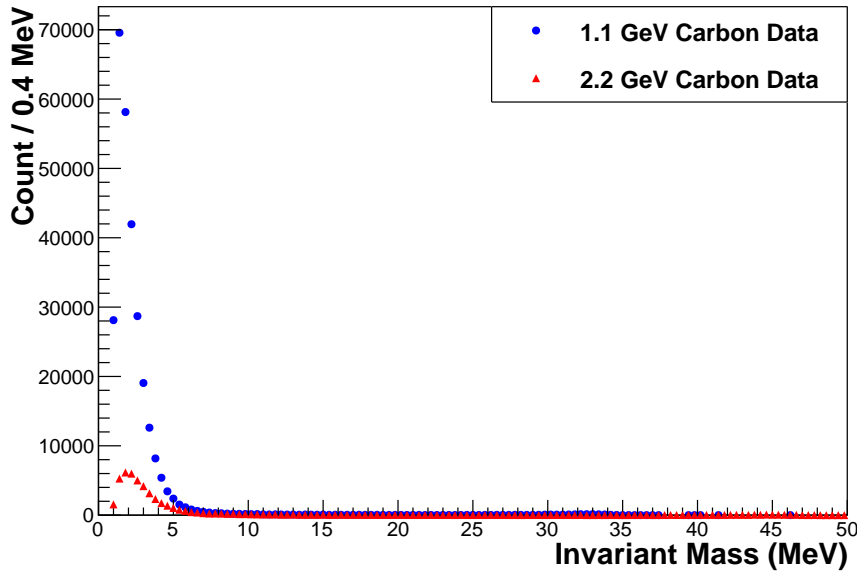


Figure 28: Invariant mass of events that pass initial event selection criteria. See the text for more information.

A tight ± 50 MeV energy conservation cut is applied to these events. With the application of this cut in Fig. 30, much of the background is removed and we see clear electromagnetic background at low invariant mass, a peak just below 10 MeV, and a peak at the high end of the invariant mass. A monte carlo simulation shows that the peak at the high end of the spectrum is consistent with what would be expected from Møller scattering off of the target. Møller scattering is a two-particle final state, so the third particle in this case is a low energy accidental.

A feature of these kinematics is that the reconstructed X momentum and the recoil electron momentum are coplanar (the recoil nucleus does not receive enough energy at these kinematics to be noticeable in this test). Figure 31 shows the $\Delta\phi$ distribution of the X -candidate and the recoil electron-candidate. There is a clear peak of events that are coplanar (180°) and a low background that are not.

By placing a $180^\circ \pm 5^\circ$ cut on the $\Delta\phi$ distribution of these events we veto events that are

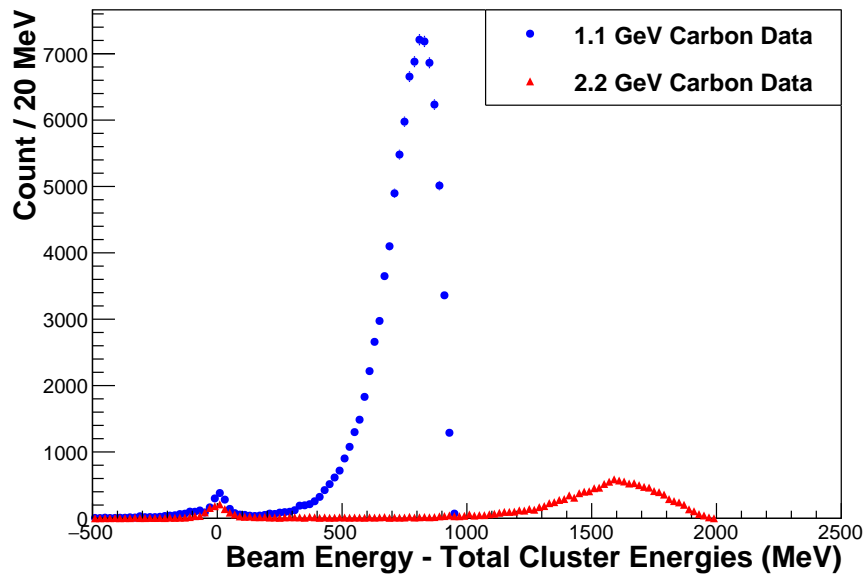


Figure 29: The difference between the beam energy and the sum of the 3 clusters that pass event selection. We can see around 0 that there is a clear peak of energy conserved events.

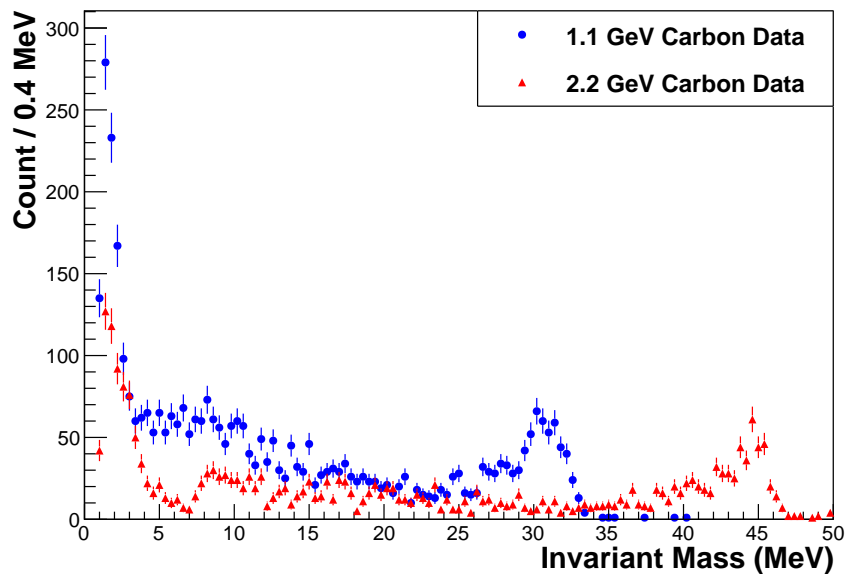


Figure 30: Invariant mass of events which pass the energy conservation cut. The peak at low invariant mass is electromagnetic background and the peak at high invariant mass is Møller scattering events with a low energy accidental.

simply 2-particle events that have a low-energy accidental third particle, such as Møller events. In those cases, because the accidental is disconnected kinematically from the rest of the event, the

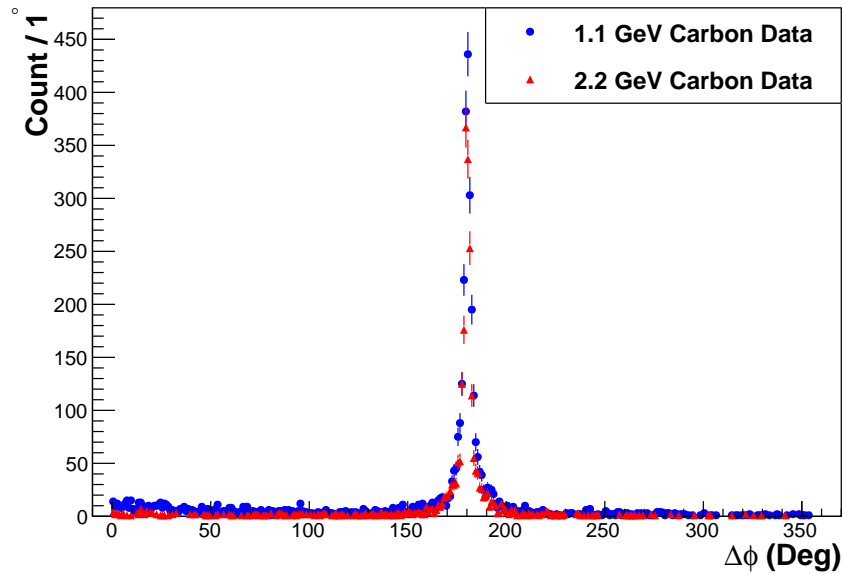


Figure 31: Coplanarity of the X -candidate and the recoil electron-candidate. The sum of the 4-momentum of the two clusters used to form the invariant mass and the 4-momentum of the third cluster should be coplanar if it truly the production of an X .

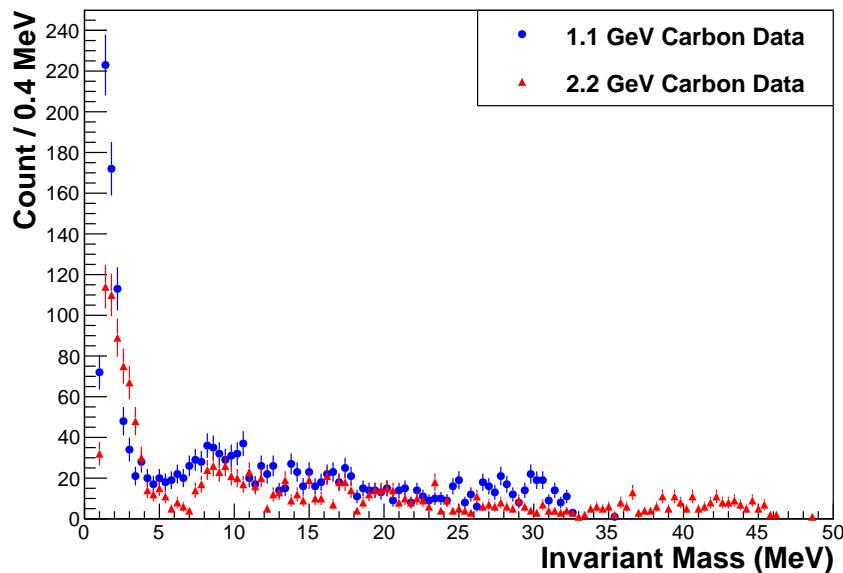


Figure 32: Invariant mass of events after applying a coplanarity cut. The Møller peak has been removed because the third cluster is an accidental that will, typically, not be coplanar with the clusters from the Møller electrons.

$\Delta\phi$ spectrum will form a smooth background rather than a sharp peak. We can see from Fig. 32 that the application of this cut has completely removed the Møller invariant mass peak.

At this point, it is curious to note that the bump just below 10 MeV has survived all of these cuts. However, when one looks closer it becomes evident that there is a slight shift in the peak placement between the 1.1 GeV and 2.2 GeV data. This highlights the need for the use of multiple beam energies. By incorporating more than one beam energy, events that do not originate from a particle decay will see a shift in their invariant mass. This is critical for avoiding misidentifying another physics process as evidence of new physics.

Finally, we took a look at a very rough tracking of the events. There is minimal distance between the GEM and HyCal which results in very poor resolution of the vertex of events. However, we can do a very rough attempt at determine the z -vertex of these events. Specifically, we look at the z position of closest approach of the two tracks that form the X invariant mass. Figure 33 shows the reconstructed z position of the vertex of events in the bump described in the last paragraph, isolated by placing a cut on the invariant mass from 6 – 12 MeV. Here, it can clearly be seen that these events do not originate from the target ($z = 0$).

This study shows that even without the optimizations we plan for the PRad experimental setup, the methodology outlined in this proposal is sound. HyCal has excellent energy resolution for selection of elastic event and determining the invariant mass of events. HyCal also has excellent position resolution for rejecting events that due not meet the coplanarity criteria. We can also see that even with poor vertex reconstruction the PRad data can determine that events do not originate from the target. The proposed experiment will have two GEM layers, separated by 10 cm. These, paired with the third hit in HyCal will provide much improved vertex resolution, making it simpler to veto non-target events.

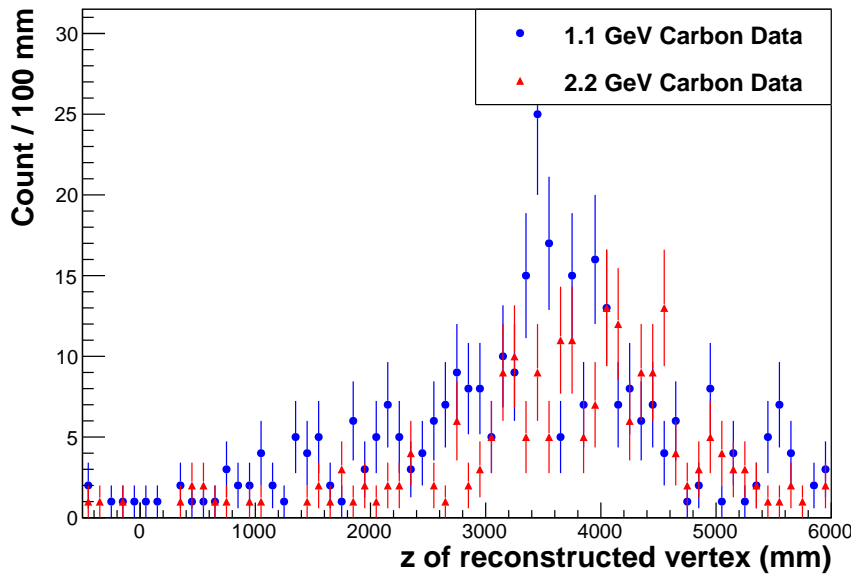


Figure 33: z -position of the reconstructed vertex of potential X events from 6 – 12 MeV, where there appears to be a peak. If the events were produced in the target, we would see a build-up around 0.

Appendix B: Additions Prior to PAC Presentation

Prior to the PAC presentation a second independent simulation was performed in order to validate the simulation of the experiment in the proposal and to respond to questions raised by various reviewers. This additional work is described below.

B.1 A second simulation using MadGraph5

To estimate the expected background level in the proposed experiment we followed the HPS procedure, (see page 48 of [43]): Note that EGS is the default generator in Geant for electromagnetic processes. We also have performed the background simulations in two different ways. As described in section 6, a comprehensive simulation of the experiment was carried out using the Geant Monte Carlo simulation package developed for this experiment. This simulation takes into account realistic geometry of the experimental setup and detector resolutions. All physical processes included in the standard Geant package had been activated and tested during these MC simulations. The results of these simulations are presented in the proposal (Fig. 24, left) as the estimated background for the beam time equivalent to 3.5 seconds. Based on this result (which is limited in statistics due to CPU time) we estimated the epsilon reach in Fig. 27. We continued these simulations and the updated results with additional statistics are presented here. As stated, the key advantage of this experiment is the detection of the 3 charged particles which arguably helps to suppress the background.

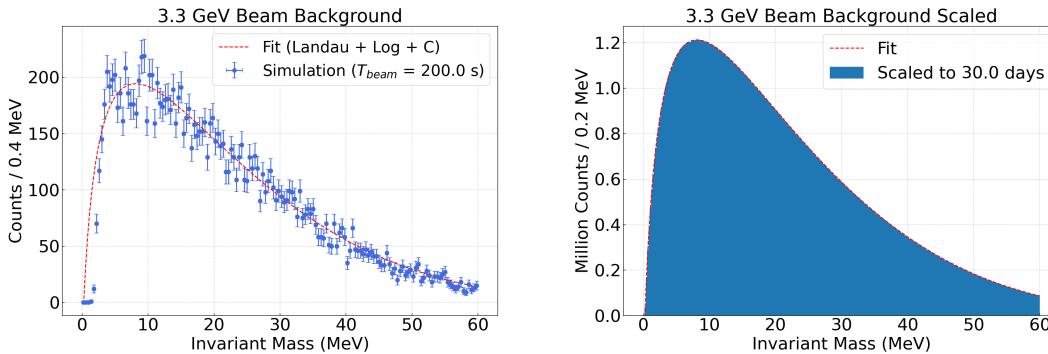


Figure 34: (Left) The MadGraph5 generated and simulated background events for the beam time equivalent to 200 s (blue points), and fitted by a sum of Landau+log+constant function (red line). (Right) Distribution of the fit result scaled to 30 days of beam time.

A second simulation was performed using the MadGraph5 event generator [44, 45], also used by the HPS collaboration [43]. First, using MadGraph5 we generated a large sample (two million events) of trident background events including the Bethe-Heitler, radiative, and interference processes. Then, these events were fed into the same Geant simulation package that was used for the signal processing to trace them through the experimental setup and detection of events. The resulting simulated background for 200 seconds of equivalent beam time is shown in Fig. 34 (left). The background shape is fit to a sum of Landau + log + constant distribution. The fit is then

used to scale the background counts to 30 days of beam time with the number of events sampled bin-by-bin, as shown in Fig. 34 (right).

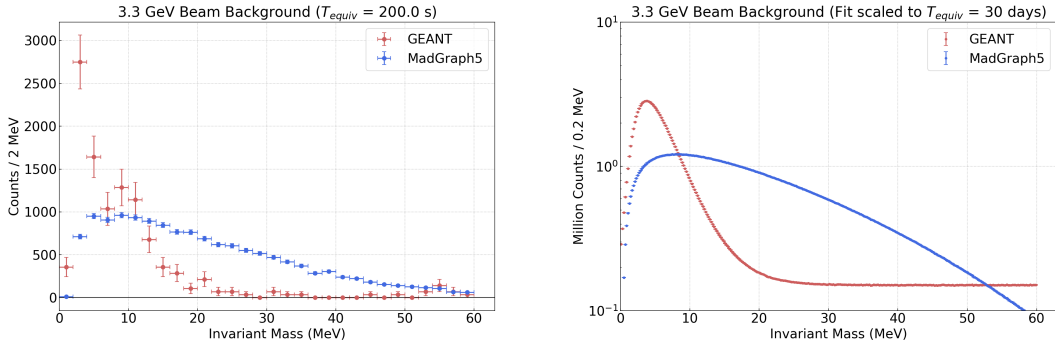


Figure 35: (Left) Comparison of the simulated background distributions performed by Geant (red points) and by MadGraph5 (blue points), they are normalized to the same 200 seconds of equivalent beam time. (Right) Distribution of fitted results scaled to the 30 days of beam time.

Fig. 35 shows comparison of the background results performed with two methods. The difference in the simulated background is $\sim 37\%$ for the integrated counts over the entire mass range (14016 vs. 10571 events). Moreover, the factor of ~ 5 difference between the two backgrounds at invariant mass of 17 MeV has a small impact on the overall coverage of the $\epsilon^2 - m_X$ phase space as shown in Fig. 36. This is very good agreement considering that Geant includes significantly more interactions than MadGraph5 uses for generating events. This agreement suggests that Bethe-Heitler and radiative trident production are the dominant source of background for this experiment.

These background distributions were used to estimate the epsilon vs. mass sensitivity. The difference in sensitivity when using the two simulations is shown in Fig. 36. This experiment defines the ϵ^2 sensitivity with a 5σ uncertainty, whereas 2-2.4 sigma is more standard in search experiments.

The formula used to estimate the ϵ sensitivity is the same one used in the APEX and HPS proposals [32, 33]. Note that it is standard practice in such search experiments to use a sensitivity limit of 2-2.4, however, we have used a sensitivity limit of 5σ (discovery criterion used by PDG), which make our estimates more conservative compared to previously approved proposals. We will develop and apply a more sophisticated statistical analysis for the actual high-statistics experimental data set.

We believe that our simulations represent a realistic expectation of the background that would be seen by this experiment with adequate precision for a hidden sector search. We are unable to use the background from other search experiments, such as HPS, as a benchmark for our expectations as the kinematics are different. Similar physics processes at the beam-target interaction region contribute to the background, but this experiment is significantly different in both tracking of produced secondary particles and their detection methods. For example, (a) both HPS and APEX are detecting the final 2 leptons only; (b) HPS (and APEX) are using magnetic field to deflect the produced leptons in their detectors. In contrast, in this proposal: (a) we require the detection of all 3 final state particles at the trigger level; and (b) we use a non-magnetic method with a calorimeter/GEM detection of the secondary particles in the very forward solid angle range.

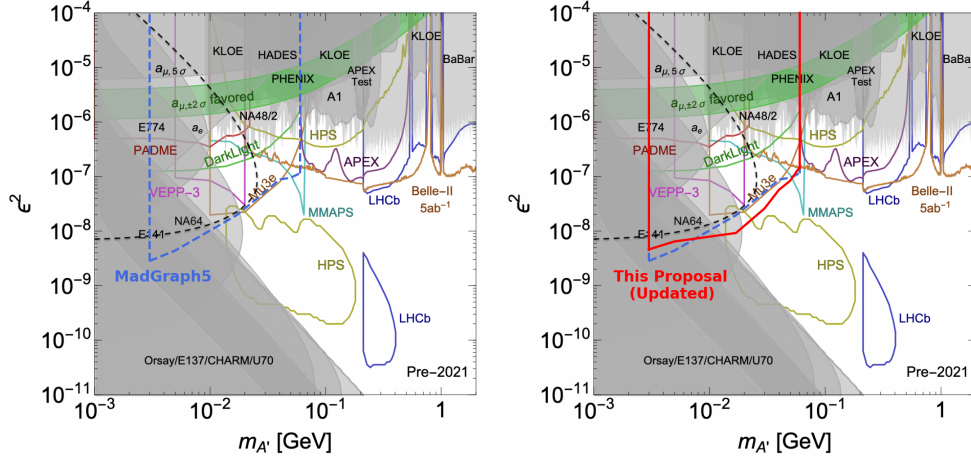


Figure 36: (Left) The $\epsilon^2 - m_X$ sensitivity for backgrounds simulated using the MadGraph5 generator. (Right) Comparison of the $\epsilon^2 - m_X$ sensitivity for backgrounds simulated using Geant (red) vs. MadGraph5 (blue) generators.

The 2-lepton detection method with a magnetic field (HPS and APEX) leaves a relatively large phase space for the production of many background channels, and, in addition, it also directs a significant amount of e^+e^- pairs produced in the target within a very narrow cone (a process with one of the largest cross sections) towards the detection aperture. The 2-lepton detection method also does not allow any energy conservation or co-planarity selection criteria to be applied. On the contrary, the proposed method is significantly less sensitive to the e^+e^- pairs produced in the target, simply allowing for most of them to pass either through the central non-sensitive part of the detectors ($12 \times 12 \text{ cm}^2$), or, if they hit the PbWO_4 calorimeter, to be rejected by the minimum shower separation criterion. Finally, the detection of all 3 particles in this proposal allows two additional selection criteria: (a) conservation of total energy in the reaction; (b) coplanarity between the scattered electron (e') and the virtual photon that produced the e^+e^- pair (a very effective selection criterion for the suppression of: (a) combinatorial background; and (b) events with higher multiplicity).

It is worth noting that the Geant simulated background shape is similar to what we find from the analysis of the PRad calibration data on a Carbon target (see Fig. 32). This level of agreement is without using any of the additional timing information which will be available in the proposed experiment but had limited availability during the PRad experiment. The comparison between the two background simulations and the analysis of the PRad calibration data on ^{12}C all conclusively demonstrate that we have made a reasonable estimate of the background.

B.2 Alternative beam energy choices

The two energies were chosen as they have high detection efficiencies within the mass region of interest and the relative ease of scheduling during the CEBAF low-energy run periods. However, we studied the acceptance of more “standard” CEBAF beam energies as well in order to have flexibility for ease of scheduling. Other reasonable choices of beam energies are possible, as can

be seen in Fig. 37 where the detection efficiency is shown for four different beam energies. As this figure shows, this experiment could alternatively run with 2.2 and 4.4 GeV beam energies.

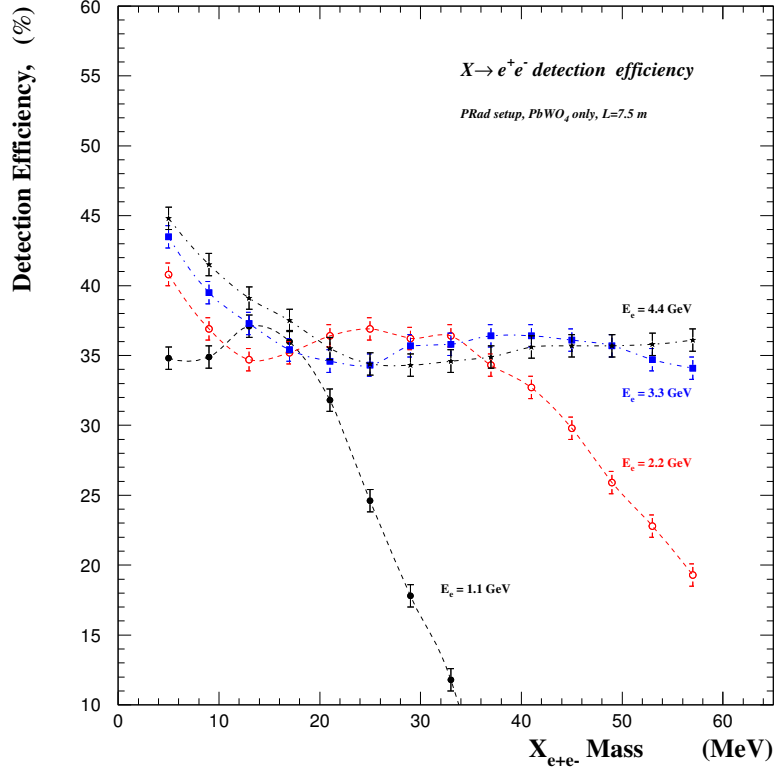


Figure 37: Detection efficiency of an $X \rightarrow e^+e^-$ decay for 1.1 GeV, 2.2 GeV, 3.3 GeV and 4.4 GeV beam energies. 1.1 GeV was not chosen due to the rapid efficiency drop at higher masses.

B.3 Further study and discussion of event selection

To ensure that we have selected our cuts in an optimal way, we studied the minimum energy cut applied to each shower in HyCal to understand how it affects our acceptance. Good energy resolution is required for all e^+e^- detection for these low-mass range particles. The energies of the decay e^+e^- pairs for beam energies in the GeV range are predominantly defined by the energy of the initial virtual photon that produced the X-particle (the Lorentz-boost effect). As an example, the energy spectra of the decay positrons from a 10 MeV particle are shown in Fig. 38 (left) for both 3.3 GeV (top) and 2.2 GeV (bottom) beam energy for a 30 MeV minimum energy cut (as described in the proposal). To demonstrate the sensitivity of the detection efficiencies to the minimum energy cut, we doubled the minimum energy cut to 60 MeV (see Fig. 38 (right)). As seen in this figure, the change in the detection efficiency is on the few percent level, mostly in the lower mass range.

This proposal plan to setup a hardware trigger from 30 MeV to 80% of the beam energy for all three (3) individual clusters energies. In addition, the hardware trigger will also select events with

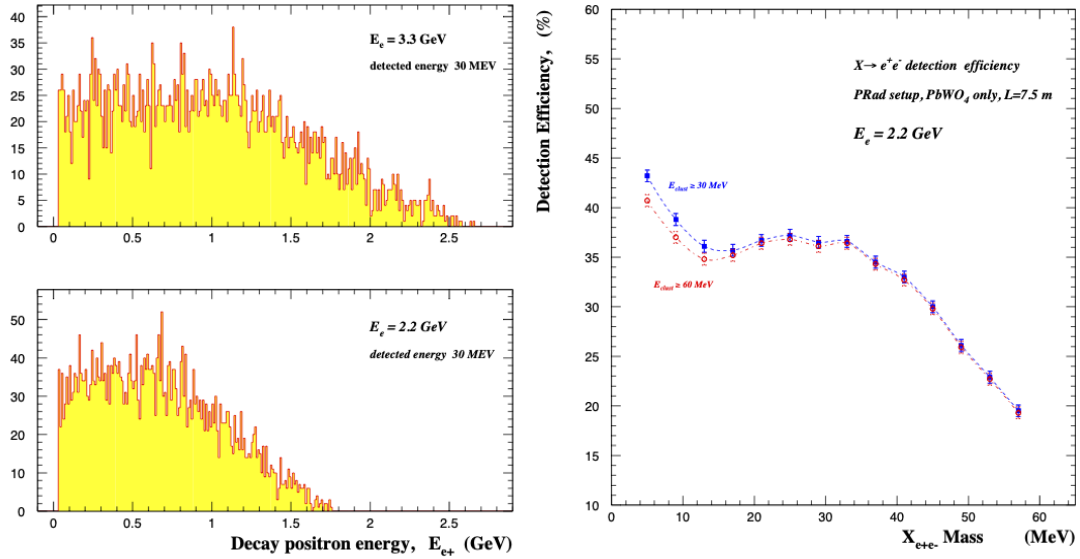


Figure 38: (left) The simulated energy spectrum of the detected positrons from the decay of a 10 MeV mass particle for a 2.2 GeV (bottom) and 3.3 GeV (top) beam energy with a 30 MeV minimum energy threshold. (right) The simulated geometrical detection efficiency as a function of e^+e^- invariant mass, for a minimum energy threshold of 30 MeV (blue) and 60 MeV (red).

total energy of three clusters greater than 70% of the beam energy. Only the central PbWO_4 part of the HyCal calorimeter will be used in this proposed experiment. We specially chose to use the crystal detectors to have a very good detection characteristics (both in energy and position) in the 30 MeV to about 3 GeV range.

The high energy and position resolution of the PbWO_4 crystals will provide very good invariant mass resolution in the [3-60] MeV mass range (Fig. 21). A very recent measurement, Ref. [46], on similar PbWO_4 crystal detectors was performed at Mainz down to the ~ 30 MeV energy range at room temperature (see Fig. 39), demonstrating the excellent performance of PbWO_4 detectors at MeV energies. Their fit: $\sigma_r(E) = \frac{2.92\%}{\sqrt{E}} + 1.18\%$ gives about 4% resolution when extrapolated to 1 GeV, which is slightly higher than measurements at higher energies carried out during the PrimEx experiment. For example, our measurements, shown in Fig. 14 and 15, performed with cooled crystals gives 2.7% at 1 GeV. The ~ 1 GeV limit on these resolutions was due to lowest energy reached by the Hall B Photon Tagger during that experiment. The authors of the Mainz measurements explain this slight difference with similar arguments about the temperature of the crystals during the measurement.

B.4 Discussion of experimental design choices

The updated DAQ is a part of the approved PRad-II experiment and the collaboration is exploring both internal JLab electronics pools to borrow for this experiments and/or external funding to upgrade the HyCal DAQ. The NIM crate system forming the trigger is one of the integral parts of the HyCal calorimeter (it is using a completely separate, the dynode signals from each shower

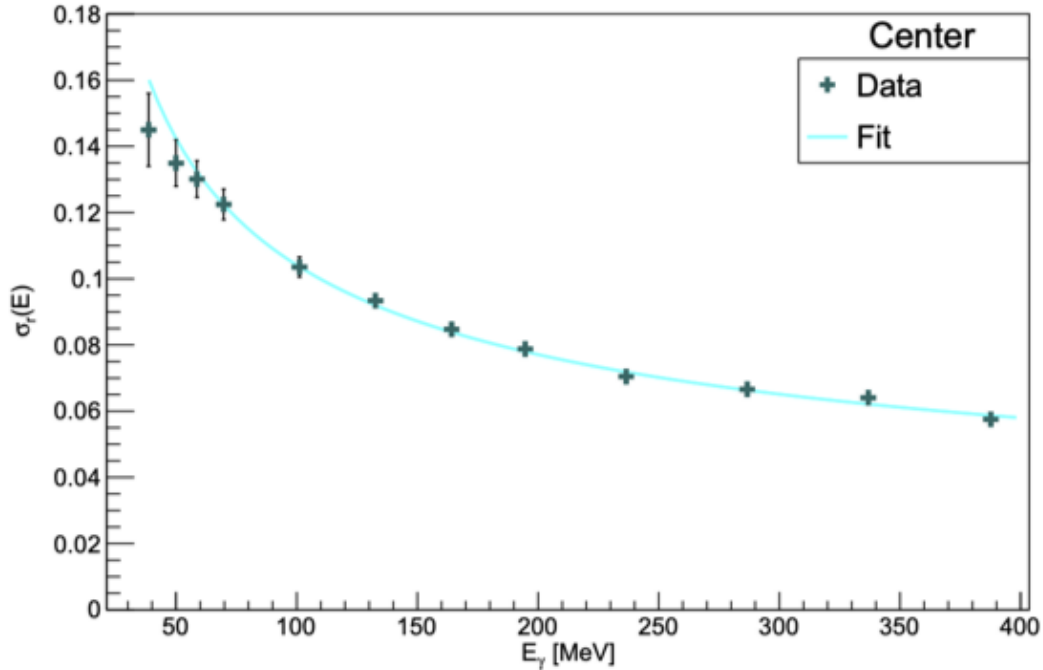


Figure 39: The measured relative resolution of the cluster energy response as function of the incident photon energy E_γ as reported by a recent Mainz experiment [46].

detector), which is why it has been left in the the presented DAQ layout. In principle, the total sum would be done with the new flash ADC system.

The PRad target chamber is proposed to be used in this experiment to be able run in sequence with the PRad-II experiment. That would keep additional costs as low as possible. If the experiment runs as a stand alone installation, an appropriate diameter beam pipe would be more practical. We also plan on addressing the poor vacuum in the large downstream chamber with additional pumps in the same manner as planned for the PRad-II experiment.

The vacuum chamber is a part of the PRad-II experiment and this proposal's experimental setup. The anticipated downtime for installation of the setup, including the vacuum chamber, will be similar to that of the previous PRad experiment (about 3 weeks). There is no significant difference in experimental configurations between the PRad-II experiment and this proposal. This is an intentional design choice so that this experiment could be run in sequence with PRad-II.

References

- [1] J. Alexander et al. Dark Sectors 2016 Workshop: Community Report. *arXiv:1608.08632*, 2016.
- [2] M. Battaglieri et al. US Cosmic Visions: New Ideas in Dark Matter 2017: Community Report. *arXiv:1707.04591*, 2017.
- [3] Tulin S. and Yu H.-B. Dark Matter Self-interactions and Small Scale Structure. *Phys. Rep.*, 730:1–57, 2018.
- [4] Bahcall N. A., Ostriker J. P., Perlmutter S., and Steinhardt P. J. The Cosmic Triangle: Revealing the State of the Universe. *Science*, 284:1481, 1999.
- [5] E. Aprile et al. Dark Matter Search Results from a One Ton-Year Exposure of XENON1T. *Phys. Rev. Lett.*, 121:111302, 2018.
- [6] R. Holdom. Two U(1)’s and Epsilon Charge Shifts. *Phys. Lett. B*, 166:196–198, 1986.
- [7] J. D. Bjorken, R. Essig, P. Schuster, and N. Toro. New Fixed-Target Experiments to Search for Dark Gauge Forces. *Phys. Rev. D*, 80:075018, 2009.
- [8] J. L. Feng, B. Fornal, I. Galon, S. Gardner, T. M. P. Smolinsky, J. and Tait, and P. Tanedo. Protophobic Fifth-Force Interpretation of the Observed Anomaly in ^8Be Nuclear Transitions. *Phys. Rev. Lett.*, 117(7):071803, 2016.
- [9] Kaplinghat M., Tulin S., and Yu H.-B. Dark Matter Halos as Particle Colliders: A Unified Solution to Small-Scale Structure Puzzles from Dwarfs to Clusters. *Phys. Rev. Lett.*, 116:041302, 2016.
- [10] T. Albahri et al. Magnetic-field measurement and analysis for the Muon $g - 2$ Experiment at Fermilab. *Phys. Rev. A*, 103(4):042208, 2021.
- [11] G. W. Bennett et al. Final Report of the Muon E821 Anomalous Magnetic Moment Measurement at BNL. *Phys. Rev. D*, 73:072003, 2006.
- [12] G. Arcadi, A. S. De Jesus, T. B. De Melo, F. S. Queiroz, and Y. S. Villamizar. A 2HDM for the $g-2$ and Dark Matter. *arXiv:2104.04456*, 2021.
- [13] P. Athron, C. Balázs, D. H. Jacob, D. Kotlarski, W. and Stöckinger, and H. Stöckinger-Kim. New physics explanations of a_μ in light of the FNAL muon $g - 2$ measurement. *arXiv:2104.03691*, 2021.
- [14] D. Borah, M. Dutta, S. Mahapatra, and N. Sahu. Muon ($g - 2$) and XENON1T Excess with Boosted Dark Matter in $L_\mu - L_\tau$ Model. *arXiv:2104.05656*, 2021.
- [15] S.-F. Ge, X.-D. Ma, and P. Pasquini. Probing the Dark Axion Portal with Muon Anomalous Magnetic Moment. *arXiv:2104.03276*, 2021.

- [16] F.W.N. de Boer, O. Fröhlich, K.E. Stiebing, K. Bethge, H. Bokemeyer, A. Balanda, A. Buda, R. van Dantzig, Th.W. Elze, H. Folger, J. van Klinken, K.A. Müller, K. Stelzer, P. Thee, and M. Waldschmidt. A deviation in internal pair conversion. *Phys. Lett. B*, 388:235–240, 1996.
- [17] F W N de Boer, R van Dantzig, J van Klinken, K Bethge, H Bokemeyer, A Buda, K A Müller, and K E Stiebing. Excess in nuclear e^+e^- pair near 9 MeV/c² invariant mass. *J. Phys. G*, 23:L85–L96, 1997.
- [18] F. W. N. de Boer, K. Bethge, H. Bokemeyer, R. van Dantzig, J. van Klinken, V. Mironov, K. A. Muller, and K. E. Stiebing. Further search for a neutral boson with a mass around 9-MeV/c². *J. Phys. G*, 27:L29, 2001.
- [19] A. J. Krasznahorkay et al. Observation of Anomalous Internal Pair Creation in Be8 : A Possible Indication of a Light, Neutral Boson. *Phys. Rev. Lett.*, 116(4):042501, 2016.
- [20] A. J. Krasznahorkay et al. New evidence supporting the existence of the hypothetical X17 particle. *arXiv:1910.10459*, 2019.
- [21] Search for new physics in e+e-final states near an invariant mass of 17 mev using the cebaf injector. http://www.jlab.org/exp_prog/proposals/20/PR12-20-001_Proposal.pdf, 2020.
- [22] X. Zhang and G. A. Miller. Can a protophobic vector boson explain the ATOMKI anomaly? *Phys. Lett. B*, 813:136061, 2021.
- [23] J. D. Bjorken et al. Search for neutral metastable penetrating particles produced in the slac beam dump. *Phys. Rev. D*, 38:3375, 1988.
- [24] E. D. Riordan et al. Search for short-lived axions in an electron-beam-dump experiment. *Phys. Rev. Lett.*, 59:755, 1987.
- [25] A. Bross et al. Search for short-lived particles produced in an electron beam dump. *Phys. Rev. Lett.*, 67:2942, 1991.
- [26] M. S. Turner. Search for short-lived particles produced in an electron beam dump. *Phys. Rev. Lett.*, 60:1797, 1988.
- [27] D. Banerjee et al. Improved limits on a hypothetical X(16.7) boson and a dark photon decaying into e^+e^- pairs. *Phys. Rev. D*, 101(7):071101, 2020.
- [28] B. Aubert et al. Search for dimuon decays of a light scalar in radiative transitions $Y(3s) \rightarrow \gamma A_0$. *arXiv:0902.2176*, 2009.
- [29] M. Pospelov. Secluded U(1) below the weak scale. *Phys. Rev. D*, 80:095002, 2009.
- [30] J. Alexander. MMAPS: Missing-Mass A-Prime Search. *EPJ Web Conf.*, 142:01001, 2017.
- [31] Research proposal for an experiment to search for the decay $\mu \rightarrow eee$. <https://www.psi.ch/sites/default/files/import/mu3e/DocumentsEN/ResearchProposal.pdf>, 2012.

- [32] Proposal to search for massive photons at jefferson laborator hps heavy photon search. https://www.jlab.org/exp_prog/PACpage/PAC37/proposals/Proposals/New%20Proposals/PR-11-006.pdf, 2011.
- [33] The $[a']$ experiment (apex):search for a new vector boson a' decaying to e^+e^- . https://www.jlab.org/exp_prog/proposals/10/PR12-10-009.pdf, 2010.
- [34] Technical proposal. <http://cds.cern.ch/record/290969>, 1994. Cover title : CMS, the Compact Muon Solenoid : technical proposal.
- [35] K. Mengel et al. *IEEE Trans. Nucl. Sci.*, 45:681–685, 1998.
- [36] Primex conceptual design report. <http://www.jlab.org/primex/>, 2000.
- [37] A proposal for the darklight experiment at the jefferson laboratory free electron laser. https://www.jlab.org/exp_prog/proposals/12/C12-11-008.pdf, 2012.
- [38] J. Balewski et al. The DarkLight Experiment: A Precision Search for New Physics at Low Energies. *arXiv:1412.4717*, 2014.
- [39] L. M. Bueno. X_{17} anomaly and prospects for its verification with NA64 experiment. *PoS, LHCP2020:177*, 2021.
- [40] L. Doria, P. Achenbach, M. Christmann, A. Denig, P. Gülker, and H. Merkel. Search for light dark matter with the MESA accelerator. *arXiv:1809.07168*, 2018.
- [41] L. Doria, P. Achenbach, M. Christmann, A. Denig, and H. Merkel. Dark Matter at the Intensity Frontier: the new MESA electron accelerator facility. *PoS, ALPS2019:022*, 2020.
- [42] M. Mihovilović et al. First measurement of proton’s charge form factor at very low Q^2 with initial state radiation. *Phys. Lett. B*, 771:194–198, 2017.
- [43] Status of the heavy photon search experiment at jefferson laboratory. https://www.jlab.org/exp_prog/proposals/12/C12-11-006.pdf, 2014.
- [44] J. Alwall, R. Frederix, S. Frixione, V. Hirschi, F. Maltoni, O. Mattelaer, H. S. Shao, T. Stelzer, P. Torrielli, and M. Zaro. The automated computation of tree-level and next-to-leading order differential cross sections, and their matching to parton shower simulations. *JHEP*, 07:079, 2014.
- [45] E. Conte, B. Fuks, and G. Serret. MadAnalysis 5, A User-Friendly Framework for Collider Phenomenology. *Comput. Phys. Commun.*, 184:222–256, 2013.
- [46] M. Erzer. Energy Response and Resolution Investigation of $PbWO_4$ Detector Elements in the tagged monochromatic Photon Beam of MAMI. https://jazz.physik.unibas.ch/site/publications/master/master_erzer.pdf, 2020. U. of Basel, Masters Thesis.